1. Report No. SWUTC/13/600451-00006-1	2. Government Accession No.	3. Recipient's Catalog No.	
4. Title and Subtitle A COMPREHENSIVE CHARACTERIZATION OF ASPHALT MIXTURES IN COMPRESSION		5. Report Date August 2013	
		6. Performing Organization Code	
7. Author(s) Yuqing Zhang, Rong Luo, and Robert L. Lytton		8. Performing Organization Report No. Report 600451-00006-1	
9. Performing Organization Name and Address Texas A&M Transportation Institute The Texas A&M University System College Station, Texas 77843-3135		10. Work Unit No. (TRAIS)	
		11. Contract or Grant No. DTRT12-G-UTC06	
12. Sponsoring Agency Name and Address Southwest Region University Transportation Center Texas A&M Transportation Institute Texas A&M University System College Station, Texas 77843-3135		13. Type of Report and Period Covered Final Report: April 2012–March 2013	
		14. Sponsoring Agency Code	
15. Supplementary Notes Supported by a grant from the U.S. Department of Transportation, University Transportation Centers Program and general revenues from the State of Texas.			

16. Abstract

Permanent deformation (i.e., rutting) is one of the major distresses in asphalt pavements, and it consists of irrecoverable deformation due to viscoplastic flow and viscofracture fatigue damage. The mechanisms of rutting have not been well addressed due to the complexities of asphalt mixture including (a) distinctions between compression, extension, and tension; (b) rate and temperature dependence; (c) dilative volumetric change; (d) frictional material with cohesion; (e) inherent anisotropy due to preferential aggregates' orientation; (f) crack-induced anisotropy due to crack growth; (g) strain hardening during viscoplastic accumulation; and (h) strain softening during viscofracture evolution.

In this project, all of the aforementioned fundamentals of asphalt mixtures were simultaneously characterized by a comprehensive viscoplastic-fracture mechanistic model, which was incorporated with (a) a modified effective stress to consider the inherent anisotropy and the crack-induced anisotropy due to viscofracture cracking in compression; (b) a smooth and convex Generalized Drucker-Prager (GD-P) yield surface; (c) a non-associated viscoplastic flow rule; (d) a rate- and temperature-dependent strain hardening rule; and (e) a viscofracture evolution that was modeled by an anisotropic damage density-based pseudo J-integral Paris' law. The model parameters were related to fundamental material properties that were measurable and understandable for civil engineers. A systemic testing protocol including five individual test methods were proposed to determine the model parameters and material properties. The test protocol was demonstrated to be efficient, as one asphalt mixture could be completely characterized within 1 day. The GD-P yield surface model was validated by octahedral shear strength tests at different normal and confining stresses. The GD-P model was able to characterize the full range of the internal friction angles from 0 to 90 degrees. In contrast, the widely used Extended Drucker-Prager (ED-P) model can only be used for a material that has an internal friction angle less than 22 degrees due to the convexity criterion of the yield surface.

17. Key Words Asphalt Mixtures, Rutting, Constitutive Modeling, Compression, Anisotropy, Viscoplasticity, Viscofracture	18. Distribution Statement No restrictions. This document is available to the public through the National Technical Information Service Alexandria, Virginia 22312 http://www.ntis.gov		
19. Security Classification (of this report) Unclassified	20. Security Classification (of this page) Unclassified	21. No. of Pages 79	22. Price

Form DOT F 1700.7 (8-72)　　　　Reproduction of completed page authorized

A Comprehensive Characterization of Asphalt Mixtures in Compression

By

Yuqing Zhang, Ph.D.
Postdoctoral Research Associate
Texas A&M Transportation Institute

Rong Luo, Ph.D., P.E.
Associate Research Engineer
Texas A&M Transportation Institute

and

Robert L. Lytton, Ph.D., P.E., Professor
Zachry Department of Civil Engineering
Texas A&M University

DISCLAIMER

The contents of this report reflect the views of the authors, who are responsible for the facts and the accuracy of the information presented herein. This document is disseminated under the sponsorship of the Department of Transportation, University Transportation Centers Program in the interest of information exchange. The U.S. Government assumes no liability for the contents or use thereof.

ACKNOWLEDGMENTS

TABLE OF CONTENTS

LIST OF FIGURES

LIST OF TABLES

EXECUTIVE SUMMARY

Permanent deformation (rutting) is one of the major distresses on asphalt pavements, and it not only increases road roughness but traps water and leads to wet-weather accidents due to loss of tire-pavement friction and hydroplaning. However, the mechanisms of rutting have not been well addressed due to the complexities of asphalt mixtures including:

- Significant distinctions between compression and tension.
- Rate-, temperature-, and aging dependent viscosity.
- Dilative volumetric change.
- Frictional material with cohesion.
- Inherent anisotropy due to inclined aggregates.
- Viscoplastic strain hardening.
- Viscofracture softening due to growth of cracks.

To accurately predict rutting in field pavements, it is crucial to comprehensively model the above fundamental material behaviors of asphalt concrete in compression. In this project, permanent deformation (rutting) was comprehensively investigated by characterizing the inherent anisotropy and viscoelasticity of undamaged asphalt mixtures and by modeling the anisotropic viscoplasticity and viscofracture cracking of damaged asphalt mixtures when they were subjected to compressive loads. A modified Perzyna's anisotropic viscoplastic-fracture model, which incorporated the following capabilities and properties, was employed:

- A modified effective stress was employed in the formulation of the models to account for both the inherent anisotropy due to the aggregates' orientation and the crack-induced anisotropy caused by crack growth. The permanent deformation of the asphalt pavement would be underestimated if the anisotropy were not included in the viscoplastic modeling of the asphalt mixture.
- A generalized Drucker-Prager (GD-P) yield surface was developed to provide a smooth and convex yield surface and to address the cohesion and internal friction of the material. The GD-P model was validated by octahedral shear strength tests at different normal and confining stresses. The GD-P model was able to characterize the full range of the internal friction angles from 0 to 90 degrees. In contrast, the widely used extended Drucker-Prager (ED-P) was shown to be applicable only for a material

that had an internal friction angle less than 22 degrees due to the convexity criterion of the yield surface.

- A non-associated flow rule was used for the viscoplastic potential to address the volumetric dilation of the asphalt mixture. The slope of the viscoplastic potential surface was found to be less than the slope of the yield surface and solely dependent on the inherent anisotropy of the asphalt mixtures.

- A temperature- and strain rate-dependent strain hardening function was proposed in the GD-P model. The results of the strength tests at different temperatures and strain rates indicated that a stiffer asphalt concrete had greater cohesion and strain hardening amplitude, both of which declined as temperature increased or strain rate decreased. The temperature and strain rate factors of the yield surface can be accurately determined solely by the peak stress of the strength tests.

- A pseudo J-integral based Paris' law in terms of damage density was proposed to characterize the evaluation of the viscofracture cracking of the asphalt mixtures under a compressive destructive load. The material constants in the Paris' law were determined and found to be highly correlated. Consistent results were obtained for different asphalt mixtures; for instance, a stiffer asphalt mixture was demonstrated to have a higher modulus, a lower phase angle, a greater flow number, and a larger n_1 value (exponent of Paris' law).

Five commonly used test methods were enwrapped as a systemic testing protocol for the determinations of material properties and model parameters of asphalt mixtures:

- Lateral surface scanning (hot-dog) test.
- Nondestructive creep/dynamic modulus test.
- Destructive dynamic modulus test.
- Uniaxial compressive strength test.
- Triaxial compressive strength test.

The above testing methods used in this study were very effective and efficient in the determinations of the model parameters and material properties. The five tests were able to be finished within 1 day given that the asphalt mixture specimens were ready for testing. Thus, by using the mechanistic models and testing protocol proposed in this project, one can characterize

one type of the asphalt mixture and obtain all the material properties and model parameters of the asphalt mixture within 1 day, which is very efficient in terms of testing time and costs.

The constitutive models developed for the characterization of asphalt concrete in compression could be effectively incorporated in the finite element modeling of asphalt pavement and used for performance prediction under a variety of traffic, structural, and environmental conditions, which is also the ongoing research work of the authors.

1. INTRODUCTION

Literature Review

A successful performance prediction model for asphalt pavement relies on a rational and comprehensive characterization of the fundamental material properties of asphalt mixtures as well as the development of a maneuverable and fast testing protocol for the accurate determination of the model parameters. Many efforts have been made to investigate permanent deformation and the associated fracture of asphalt mixtures for decades. Multiple theories and methods have been employed including phenomenological empirical methods (Perl et al., 1983; Mahboub, 1990; Uzan, 1996; Qi and Witczak, 1998) and mechanistic theories that consist of viscoelastic damage models (Sousa et al., 1993; Ramsamooj and Ramadan, 1999) and elasto-viscoplastic damage models (Chehab et al., 2003; Schwartz et al., 2004; Nguyen et al., 2007; Darabi et al., 2011). The models that use mechanistic constitutive equations to model material characteristics utilize the fundamental engineering properties of materials as inputs and can be applied to different types of materials in a variety of pavement structures, traffic, and environmental conditions. Thus, the mechanistic models, especially the viscoelastic-viscoplastic-damage model, are becoming more appealing to researchers as well as to civil engineers.

Examples of these mechanistic models are presented as follows. Sousa et al. (1993) and Sousa and Weissman (1994) proposed a nonlinear viscoelastic damage model to predict the permanent deformation of an asphalt mixture that included a volumetric component accounting for densification of air voids and a deviatoric component responsible for a softening or hardening process. Florea (1994a; 1994b) developed an associated and a non-associated viscoplastic model to describe the mechanical properties of asphalt mixtures. Schapery (1997; 1999) employed thermodynamic principles incorporated with internal state variables to develop the constitutive relations that account for the effects of viscoelasticity, viscoplasticity, growing damage, and aging. Based on Schapery's viscoplastic continuum model, Gibson et al. (2003) investigated the properties of asphalt mixtures in an unconfined compressive state, and Chehab et al. (2003) predicted the responses of asphalt mixtures in a uniaxial tensile condition. Other researchers (Huang et al., 2007; Saadeh et al., 2007; Masad et al., 2008; Darabi et al., 2011) employed Schapery's nonlinear viscoelastic model (Schapery, 1969) and Perzyna's viscoplastic model (Perzyna, 1971) associated with a damage density function to characterize the properties of asphalt mixtures and predicted pavement performance based on finite element simulations.

1

Nevertheless, due to the complicated behaviors of asphalt mixtures, the existing mechanistic models are far from being widely used because of some problems in the models themselves; for example, they cannot characterize permanent deformation and cracking simultaneously, and difficulties exist in acquiring the fundamental engineering material properties required by the models. Another limitation of the existing constitutive models is the ability to account for the anisotropy of asphalt mixtures. The anisotropy of asphalt mixtures includes inherent anisotropy that results from horizontally preferential oriented aggregates and crack-induced anisotropy that is caused by direction-dependent crack growth. Few mechanistic analyses have taken into account the anisotropic effect, which has led to unreasonable prediction of permanent deformation and cracking of asphalt pavements.

Therefore, the following aspects need more research efforts:

- Anisotropy including inherent anisotropy and crack-induced anisotropy must be accounted for in the constitutive modeling of asphalt mixtures. Otherwise, permanent deformation and cracking will be underestimated if using the assumption of asphalt mixtures being isotropic in compression.

- A more comprehensive constitutive model is needed to characterize a variety of the viscoplastic-viscofracture properties of asphalt mixtures in compression including the hydrostatic-dependent yield surface, the plastic potential based on a non-associated flow rule, the viscoplastic strain hardening, and the anisotropic viscofracture effect.

- A systematic testing protocol and analyzing formulations are required to rapidly and accurately determine the parameters of the constitutive model. The model parameters need to be related to the measurable and understandable material engineering properties so that civil engineers can understand the models and employ the more accessible laboratory apparatuses to conduct the material performance evaluation with using the proposed models.

Research Objectives

The objective of this study was to provide pavement engineers and researchers with fundamental mechanistic models and efficient, reliable, and user-friendly testing methods to comprehensively characterize the engineered properties of the asphalt mixtures in compression and to promote the understandings and the predictions of the pavement distresses in the field. More specifically, the following research objectives were undertaken:

- Model the constitutive behaviors of asphalt mixtures using a comprehensive equation that accounts for viscoplasticity, viscofracture, and anisotropy including inherent anisotropy and crack-induced anisotropy.
- Develop a systematic testing protocol and analyze formulations to rapidly and accurately determine the parameters of the constitutive model and relate the parameters of the constitutive model to the measurable and understandable engineering material properties.
- Investigate permanent deformation and cracking simultaneously using the proposed mechanistic model, which includes the mutually promotive effects of the two damages and the effects of binder type, air void content, and aging on the evolution of damages.

Research Tasks

The research objectives were accomplished through performing the following tasks:

- Perzyna's viscoplastic model was employed as a basic modeling framework that was formulated based on modified effective stress to consider the effects of anisotropy and viscofracture on the evolution of the damages including permanent deformation and cracking. A non-associated plastic potential function and a strain hardening law were incorporated in the anisotropic viscoplastic-viscofracture model.
- A new yield surface function was proposed to address the hydrostatic stress-dependent yield surface as well as the differences of yielding between compression and extension. The new yield surface satisfies the convex requirement and simultaneously allows the internal friction angle of asphalt mixtures to range from 0 to 90 degrees.
- A systematic testing protocol and analyzing formulations were proposed to rapidly and accurately determine the parameters of the constitutive model using commonly accessible testing equipment. In addition, to make the model understandable to civil engineers, some of the model coefficients were derived to be related to commonly used and understandable engineering material properties such as modulus, cohesion, and internal friction angle.
- Laboratory experiments according to the proposed testing protocol were performed on a variety of asphalt mixtures with different volumetric and aging properties, and

mechanical tests were proposed and performed to validate the proposed yield surface model and the strain hardening model for asphalt mixtures. The variables of the tested asphalt mixtures included two types of binders, two air void contents, and three aging periods.

This final report summarizes the proposed constitutive model, characterizing test protocol, theoretical analysis, data analysis methods, experimental results, and findings. The report is organized into five chapters. This chapter has introduced the challenge of modeling asphalt mixtures in compression. Chapter 2 proposes a comprehensive constitutive model to account for the anisotropy, viscoplasticity, and viscofracture of asphalt mixtures. Chapter 3 describes the development of the laboratory test protocol and the data analysis methods that were employed to accurately and efficiently determine the material properties and model parameters. Chapters 4 discusses the testing results for different types of asphalt mixtures and validates the proposed viscoplastic models using the laboratory mechanistic tests. Chapter 5 summarizes the research findings and suggests future work for the modeling of asphalt mixtures.

2. ANISOTROPIC VISCOPLASTIC-FRACTURE CONSTITUTIVE MODELS FOR ASPHALT MIXTURES

A modified Perzyna's viscoplastic model was employed for the constitutive modeling of asphalt mixtures and incorporated (a) modified effective stresses in the formulation of the model to account for the inherent anisotropy and the crack-induced anisotropy; (b) a new viscoplastic yield surface to provide a smooth and convex yield surface and address the cohesion and internal friction; (c) a non-associated flow rule to address the volumetric dilation; and (d) a temperature- and strain rate-dependent strain hardening function.

Characterization of Anisotropy Using Modified Effective Stress

Inherent Anisotropy

Studies (Pickering, 1970; Tobita and Yanagisawa, 1992) on geomaterials have indicated that without consideration of inherent anisotropy caused by the preferentially oriented granular particles (e.g., soils, sands, and aggregates) in the constitutive formulation, some important material properties such as non-coaxial and dilation will not be properly accounted for. Constitutive models based on modified stresses have successfully captured the material anisotropic property where the modified stresses were obtained by modifying the nominal stress with a fabric tensor (Oda and Nakayama, 1989; Tobita, 1989). It has also been suggested that the isotropic yield condition in terms of the modified stresses can lead to the anisotropic yielding and hardening nature of granular materials with less mathematical complexities, as only the isotropic material constants are needed (Tobita and Yanagisawa, 1988).

As a granular material, asphalt concrete exhibits inherent anisotropy due to inclined aggregates that tend to be oriented along the horizontal direction. Pavement researchers (Masad et al., 1998; Tashman et al., 2002) adopted the same fabric tensor concept to account for the anisotropy during the viscoplastic constitutive modeling of asphalt concrete. The authors (Zhang et al., 2011) improved the fabric tensor using a modified vector magnitude (Δ') that considered not only aggregate orientation but also the size and shape of both coarse and fine aggregates. A high correlation was obtained between Δ' and the anisotropic modulus ratio of asphalt concrete. The modified fabric tensor is written as:

$$[F'_{ij}] = \frac{1}{3+\Delta'} \begin{bmatrix} 1-\Delta' & 0 & 0 \\ 0 & 1+\Delta' & 0 \\ 0 & 0 & 1+\Delta' \end{bmatrix} \tag{1}$$

where Δ' is the modified vector magnitude that is determined as:

$$\Delta' = \frac{1}{A_0} \sqrt{\left(\sum_{k=1}^{M} \rho^{(k)} \lambda^{(k)} \sin 2\theta_k \right)^2 + \left(\sum_{k=1}^{M} \rho^{(k)} \lambda^{(k)} \cos 2\theta_k \right)^2} \tag{2}$$

where $A_0 = \sum_{k=1}^{M} \left(\rho^{(k)} \lambda^{(k)} \right)$; and $\rho^{(k)}, \lambda^{(k)}$, and θ_k are area, aspect ratio, and inclination angle of

an aggregate, respectively, and can be accurately and quickly measured by a lateral surface

scanning test (Zhang et al., 2011). Δ' theoretically ranges between 0 and 1, where $\Delta' = 0$

indicates an isotropic condition and $\Delta' = 1$ implies a fully cross-anisotropic condition.

A modified stress tensor is introduced to combine the stress tensor and the fabric tensor

as follows (Tobita and Yanagisawa, 1988; Oda, 1993; Yang et al., 2008):

$$\bar{\sigma}_{ij} = \frac{1}{6} \left(\sigma_{in} F'^{-1}_{nj} + F'^{-1}_{in} \sigma_{nj} \right) \tag{3}$$

where, $\bar{\sigma}_{ij}$ is the modified stress tensor that considers inherent anisotropy; σ_{ij} is the nominal

stress tensor; and F'^{-1}_{ij} is the inverse of the modified fabric tensor. If a fourth-order fabric tensor

is defined as:

$$F_{imnj} = \frac{1}{6} \left(\delta_{im} F'^{-1}_{nj} + F'^{-1}_{im} \delta_{nj} \right) \tag{4}$$

where, δ_{ij} is the Kronecker delta tensor, the modified stress becomes:

$$\bar{\sigma}_{ij} = F_{imnj} \sigma_{mn} \tag{5}$$

In this study, the stresses were modified by the fabric tensor and indicated by a head bar.

The following proposed models employ the modified stress to account for the inherent

anisotropy of asphalt concrete.

Crack-Induced Anisotropy

Once cracks are initiated in a material, the load is transferred or carried out by the

remaining undamaged (effective or intact) material. The cracked (lost) area cannot transfer load

inside of the material. Thus, the constitutive relations of the damaged material should not be

formulated in terms of the apparent (nominal) stress that is calculated based on the total material

area, which includes both the intact area and the lost area. Instead, the true (effective) stress that acts only on the intact material should be used in the constitutive models of the material.

The true stress concept was introduced (Kachanov, 1986; Lemaitre and Desmorat, 2005) into continuum damage mechanics to capture the overall fracture properties of the hundreds of thousands of microcracks and macrocracks that are randomly dispersed in the damaged materials. The true stress (σ^T) is related to the apparent stress (σ^A) as follows:

$$\sigma^T = \frac{\sigma^A}{1-\xi} \tag{6}$$

where ξ is damage density. The damage density is physically defined as a ratio of the lost area due to cracks to the total area of a cross section in a specific direction (Rabotnov, 1969; Lemaitre and Desmorat, 2005; Sullivan, 2008).

Current studies (Darabi et al., 2011; Abu Al-Rub et al., 2012) assumed that the damage density is an isotropic variable for asphalt mixtures. However, the three-dimensional cracks show different projected areas in different directions, which results in different lost area ratios to the total area in orthogonal directions. Thus, the damage density is an anisotropic parameter, and it has different values and evolution velocities in different directions, which is the case when an asphalt mixture is subjected to a destructive compression load. In this study, the damage density was assigned as a cross-anisotropic parameter and defined as follows:

$$\xi_{ij} = \begin{bmatrix} \xi_1 & 0 & 0 \\ 0 & \xi_2 & 0 \\ 0 & 0 & \xi_2 \end{bmatrix} = \begin{bmatrix} A_1^L/A_1^T & 0 & 0 \\ 0 & A_2^L/A_2^T & 0 \\ 0 & 0 & A_2^L/A_2^T \end{bmatrix} \tag{7}$$

where ξ_1 and ξ_2 are axial and radial damage density, respectively; A_1^L and A_2^L are projected lost area in the axial and radial directions, respectively; and A_1^T and A_2^T are total area in the axial and radial directions, respectively.

In order to formulate the true stress tensor based on the anisotropic damage densities, a symmetric fourth-order damage density tensor is developed as follows:

$$M_{imnj} = \frac{1}{2}\left[\delta_{im}\left(\delta_{nj} - \xi_{nj}\right)^{-1} + \left(\delta_{im} - \xi_{im}\right)^{-1}\delta_{nj} \right] \tag{8}$$

where M_{imnj} is the fourth-order damage density tensor; and δ_{ij} is the Kronecker delta tensor. Then, the true (effective) stress tensor (σ_{ij}^T) becomes:

$$\sigma_{ij}^{T} = M_{imnj}\sigma_{mn}^{A} = \frac{1}{2}\left[\sigma_{in}^{A}\left(\delta_{nj} - \xi_{nj}\right)^{-1} + \left(\delta_{im} - \xi_{im}\right)^{-1}\sigma_{mj}^{A}\right] \tag{9}$$

where σ_{mn}^{A} is the apparent stress tensor. The true stress tensor is capable of accounting for the crack-induced anisotropy of the asphalt mixtures by applying the true stress tensor and the anisotropic damage densities in the constitutive modeling of the material.

To derive the axial damage density, a balance principle of the incremental dissipated pseudo fracture strain energy ($\Delta DPFSE$) is implemented between the apparent configuration and the true configuration. The details of the energy balance principle and the derivations of the axial damage density have been discussed in a preliminary study in detail (Zhang et al., 2012c). The axial damage density is determined as:

$$\xi_{1}(N) = 1 - \left[\left(\frac{1}{1 - \xi_{01}}\right)^{2} + \frac{\Delta\varepsilon_{1}^{vf}(N)}{\sigma_{0}^{A}}\frac{E_{Y}}{\pi\sin(\delta - \varphi_{II})}\right]^{-\frac{1}{2}} \tag{10}$$

where $\Delta\varepsilon_{1}^{vf}(N)$ is the increment of viscofracture strain within one load cycle; E_{Y} is Young's modulus; σ_{0}^{A} is the amplitude of the apparent repeated stress applied in the test; σ_{N}^{T} is the amplitude of the true stress at the Nth load cycle; ξ_{01} is the initial axial damage density that occurs at the flow number; δ is the phase angle of the undamaged asphalt mixture; and φ_{II} is the secondary stage phase angle of the damaged asphalt mixture.

The radial damage density is determined based on the axial and radial viscofracture strains as well as the axial damage density, which is expressed as:

$$\xi_{2} = \frac{\left(1 + \varepsilon_{2}^{vf}\right)^{2}\left(1 - \varepsilon_{1}^{vf}\right) - 1}{\sqrt{\xi_{1}}} \tag{11}$$

In this research study, a variable with a superscript (*e*) indicated that the variable had been modified by the anisotropic damage density and had become an effective (true) variable. The effective variable was used in the viscoplastic modeling to account for the crack-induced anisotropy of the asphalt mixture. If the inherent and crack-induced anisotropy needed to be accounted for simultaneously in the constitutive modeling, the following stress expression was employed to compute a modified effective stress that was used in the formulations of the constitutive relations:

$$\bar{\sigma}_{ij}^{e} = M_{imnj}F_{mabn}\sigma_{ab} \tag{12}$$

Anisotropic Viscoplastic-Fracture Constitutive Model

An anisotropic viscoplastic-fracture constitutive model is presented in this section including the Perzyna's viscoplastic flow rule, a new viscoplastic yield surface, a viscoplastic potential surface, a temperature- and strain rate-dependent strain hardening model, and the evolution rule of the viscofracture in terms of damage density.

Viscoplastic Flow Rule

The viscoplastic strain is associated with the permanent deformation of the asphalt mixture, and the rate of the viscoplastic strain can be defined by a Perzyna-type viscoplasticity theory as (Perzyna, 1971):

$$\dot{\varepsilon}_{ij}^{vp} = \Gamma \left\langle \Phi(f) \right\rangle^N \frac{\partial g}{\partial \sigma_{ij}^e} \tag{13}$$

where $\dot{\varepsilon}_{ij}^{vp}$ represents the rate of the viscoplastic strain with respect to time, Γ is the viscosity-related parameter, $1/\Gamma$ is proportional to the viscosity of the asphalt mixture, and $1/\Gamma$ also represents the viscoplastic relaxation time. Thus, Γ is a temperature-dependent parameter. N is the viscoplastic rate-dependent exponent. Both Γ and N are experimentally determined, and $N > 1$ for the asphalt mixtures. Φ is the overstress function, which is expressed in terms of the yield surface function, f. σ_{ij}^e is the effective stress tensor and is defined in Equation 9. g is the anisotropic viscoplastic plastic potential function. The non-associated flow rule applies when $g \neq f$, which is appropriate for the asphalt mixture. It must be noted that the functions of f and g are formulated by the modified effective stress $\bar{\sigma}_{ij}^e$, while the effective stress σ_{ij}^e (neither the modified effective stress $\bar{\sigma}_{ij}^e$ nor the nominal stress σ_{ij}) is utilized in the term of $\partial g / \partial \sigma_{ij}^e$ of the viscoplastic model because it is the effective stress σ_{ij}^e acting on the intact material area that drives the viscoplastic deformation of the material. The McCauley brackets in Equation 13 imply that:

$$\left\langle \Phi(f) \right\rangle = \begin{cases} 0, & \Phi(f) \leq 0 \\ \dfrac{f}{Pa}, & \Phi(f) > 0 \end{cases} \tag{14}$$

Equations 13 and 14 indicate that the viscoplastic strain occurs only when the overstress function Φ is greater than zero. The Perzyna-type viscoplastic model as shown in Equations 13

and 14 has been used to describe the viscoplastic evolution of asphalt mixtures for decades (Abdulshafi and Majidzadeh, 1984; Tan et al., 1994; Seibi et al., 2001; Tashman et al., 2005; Masad et al., 2007; Abu Al-Rub et al., 2012). However, most of the yield surface functions used in the literature studies are Drucker-Prager (D-P) or extended Drucker-Prager (ED-P) models, even though they have some significant limitations, such as non-convexity when the internal frictional angle is greater than 22 degrees. Thus, a Generalized Drucker-Prager (i.e., GD-P) yield surface model is described in the next section.

Viscoplastic Yield Surface

The GD-P yield surface function for asphalt concrete is proposed as:

$$f = \sqrt{\bar{J}_2^e} \, \rho(\theta') - \alpha \bar{I}_1^e - \kappa a_T a_{\dot{\varepsilon}} \tag{15}$$

where $\bar{J}_2^e \; (= \tfrac{1}{2} \bar{S}_{ij}^e \bar{S}_{ji}^e)$ is the second invariant of the modified effective deviatoric stress tensor $\bar{S}_{ij}^e \, (= \bar{\sigma}_{ij}^e - \tfrac{1}{3} \delta_{ij} \bar{I}_1^e)$; $\bar{I}_1^e \, (= \bar{\sigma}_{kk}^e)$ is the first invariant of the modified effective stress tensor $(\bar{\sigma}_{ij}^e)$ that is defined in Equation 12; and θ' is the Lode angle that is expressed using invariants of the modified effective stress as follows:

$$\theta' = \frac{1}{3} \arccos \left[\frac{3\sqrt{3}}{2} \frac{\bar{J}_3^e}{\left(\bar{J}_2^e \right)^{3/2}} \right] \qquad \in \left[0, \; \frac{\pi}{3} \right] \tag{16}$$

where $\bar{J}_2^e$ and $\bar{J}_3^e = \det\left(\bar{S}_{ij}^e \right)$ are the second and third invariants of the modified effective deviatoric stress tensor. θ' is zero in compression, and θ' is $\pi/3$ in extension. $\rho(\theta')$ is a function that defines the yield surface shape on the octahedral plane and determines the convexity of the yield surface, which is derived as:

$$\rho(\theta') = \mu \cos \left[\frac{1}{3} \arccos\left(\gamma \cos 3\theta' \right) \right] \tag{17}$$

where μ and γ are dependent on the extension ratio (*d*), and:

$$\begin{cases} \mu = \dfrac{2\sqrt{1-d+d^2}}{\sqrt{3}d} \\[2mm] \gamma = -\dfrac{3\sqrt{3}}{2}\dfrac{(1-d)d}{\left(1-d+d^2\right)^{3/2}} \\[2mm] d = \dfrac{3-\sin\phi}{3+\sin\phi} \end{cases} \tag{18}$$

where d is the extension ratio that is the ratio of the yield strength in extension to that in compression. ϕ is the internal friction angle of the asphalt mixture. The formula of $\rho(\theta')$ in Equation 17 ensures that the yield surface of the asphalt mixture is smooth and convex on both the meridian plane and the octahedral plane.

The GD-P model is a very general yield surface model. When the differences between extension and compression are neglected (i.e., $d=1$ and $\rho(\theta,d)=1$), the GD-P model is reduced to the Drucker-Prager model; when the cohesion is neglected ($\kappa=0$), the GD-P model becomes the Matsuoka-Nakai model. In addition, the GD-P model also satisfies the three requirements of Lode dependence for pressure-sensitive materials (Bardet, 1990): (a) extension ratio ($\rho(0)/\rho(\frac{\pi}{3})=d$ according to Equation 23); (b) smoothness ($g'(0)=g'(\frac{\pi}{3})=0$); and (c) convexity that is inherited from the Matsuoka-Nakai model.

Figure 1 plots three-dimensional GD-P yield surfaces, and Figure 2 shows the yield surface of the GD-P model on the octahedral plane with different internal friction angles. The GD-P model always provides a smooth and convex yield surface when the internal friction angle varies from 0 to 90 degrees. The extensive yield strength is less than the compressive yield strength, which is quantified by the parameter d. In fact, it can be proved that the GD-P yield surface coincides with the apices of the Mohr-Coulomb yield surface on the octahedral plane. Thus, the GD-P model can be regarded as a smoothed Mohr-Coulomb yield surface, which also considers the anisotropy, strain hardening, temperature effects, and strain rate effects. The slope and the intercept of the GD-P model can be related to Mohr-Coulomb parameters as follows:

$$\alpha = \frac{2\sin\phi}{\sqrt{3}(3-\sin\phi)} \tag{19}$$

$$\kappa_0 = \frac{6C\cos\phi}{\sqrt{3}(3-\sin\phi)} \tag{20}$$

11
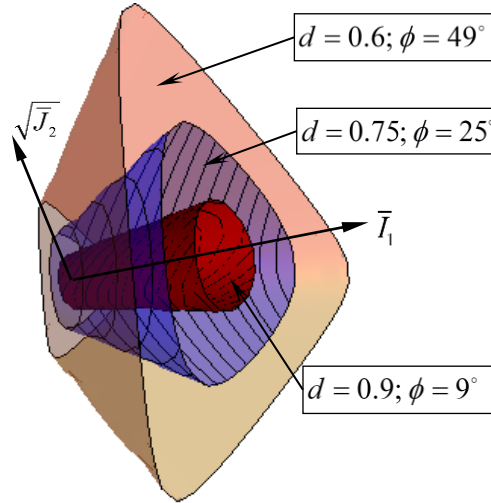
Figure 1. Generalized Drucker-Prager yield surfaces.
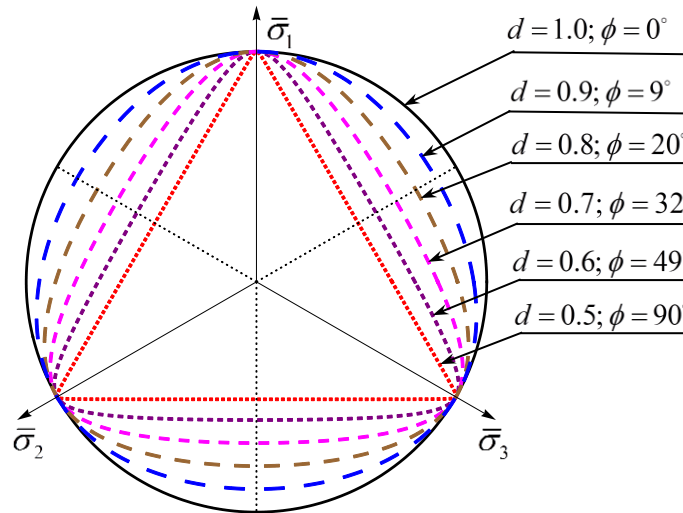
Figure 2. GD-P yield surfaces on octahedral plane.

Strain Hardening Model

The yield surface of the asphalt mixture expands with the increase of the effective viscoplastic strain, which indicates a strain hardening process. The term $\kappa a_T a_{\dot{\varepsilon}}$ in the GD-P yield surface represents the temperature- and strain rate-dependent cohesion and strain hardening for an asphalt mixture. κ is a strain hardening function that is defined by Equation 21. a_T and $a_{\dot{\varepsilon}}$ are temperature and strain rate effect factors, which are defined by Equation 22 and 23, respectively.

$$\kappa = \kappa_0 + \kappa_1 \left[1 - \exp\left(-\kappa_2 \varepsilon_e^{vp} \right) \right] \tag{21}$$

$$a_T = \exp\left[\frac{\Delta E_T}{R} \left(\frac{1}{T} - \frac{1}{T_0} \right) \right] \tag{22}$$

$$a_{\dot{\varepsilon}} = \left(\frac{\dot{\varepsilon}}{\dot{\varepsilon}_0} \right)^{\kappa_3} \tag{23}$$

where κ_0, κ_1, and κ_2 are material parameters identified at the reference temperature (T_0) and the reference strain rate ($\dot{\varepsilon}_0$); ε_e^{vp} is the effective viscoplastic strain; ΔE_T is the activation energy of the temperature effect, J/mol; R is the universal gas constant, 8.314 J/mol·K; T is the temperature of interest, K; $\dot{\varepsilon}$ is the strain rate of interest; and κ_3 is a material property that is determined by experiments.

The effective viscoplastic strain has different expressions when different yield surfaces and flow rules are used. For instance, when the von Mises yield surface and associated flow rule are used, the incremental effective plastic strain is given as $d\varepsilon_e^p = \sqrt{2/3 \, d\varepsilon_{ij}^p d\varepsilon_{ij}^p}$, where $d\varepsilon_{ij}^p$ is the incremental plastic strain tensor. The generalized expression of ε_e^{vp} is determined based on an viscoplastic work equivalence principle (Chen and Han, 1988), which states that the viscoplastic work increment ($\dot{W}_{vp}$) of a material under multiaxial loading that is expressed by the stress and strain measured on the material is equivalent to the viscoplastic work increment of the same material under uniaxial loading that is expressed by the effective viscoplastic stress (σ_e^{vp}) and the effective viscoplastic strain (ε_e^{vp}). The rate of the effective viscoplastic strain is derived as:

$$\dot{\varepsilon}_e^{vp} = \left[\left(\frac{1 - \sqrt{3}\beta}{1 - \sqrt{3}\alpha} \right)^2 + (n' - 1) \left(\frac{1 - \Delta'}{1 + \Delta'} \right)^2 \left(\frac{0.5 + \sqrt{3}\beta}{1 - \sqrt{3}\alpha} \right)^2 \right]^{-\frac{1}{2}} \sqrt{\dot{\varepsilon}_{ij}^{vp} \dot{\varepsilon}_{ij}^{vp}} \tag{24}$$

where $n' = 1$ in a uniaxial condition and $n' = 3$ in a triaxial condition. Integrating Equation 24 over time can give the effective viscoplastic strain.

Viscoplastic Potential Surface

The viscoplastic model in Equation 13 uses a non-associated viscoplastic flow rule for the asphalt mixture, which is reasonable because (a) the associated flow rule would overestimate

the amount of viscoplastic dilation of materials, and (b) the direction of the viscoplastic strain increment is not perpendicular to the yield surface but to the viscoplastic potential surface. It is assumed that the viscoplastic potential surface has the same linear form as the yield surface but with a smaller slope, which affects the volumetric dilation of the material. Thus, the viscoplastic potential is expressed as:

$$g = \sqrt{\bar{J}_2^e} \, \rho(\theta') - \beta \bar{I}_1^e - \kappa_4 \tag{25}$$

where β is the slope of the viscoplastic potential surface and $\beta \neq \alpha$. κ_4 is the incept of the viscoplastic potential surface, which vanishes during the calculation of $\partial g / \partial \sigma_{ij}^e$. A number of studies have indicated that the value of β is less than the value of α for geomaterials such as soils, sands, and asphalt mixtures (Oda and Nakayama, 1989; Tashman et al., 2005).

A normality condition must be satisfied in that the viscoplastic stain increment is normal to the viscoplastic potential surface. Based on this, the slope of the viscoplastic potential function is derived to have the following relation:

$$\beta = \frac{\sqrt{3}\left(Xa + 2Yb\right)}{Yb - Xa} = \frac{2\Delta' - 3\sqrt{3}\beta + \sqrt{3}\beta\Delta'}{-\frac{\sqrt{3}}{2} - \frac{\sqrt{3}}{6}\Delta' + 2\beta\Delta'} \tag{26}$$

Equation 26 is an implicit solution for β. Thus, for practical use, the values of β are resolved over the entire theoretical range of Δ' from 0 to 1. Then, a linear relationship is regressed with a high coefficient of determination (R^2) as follows:

$$\beta = 0.5889\Delta' - 0.0122 \ \left(R^2 = 0.9988\right) \tag{27}$$

For the asphalt mixture, Δ' normally ranges from 0.2 to 0.5. Thus, β changes from 0.1 to 0.28 according to Equation 27. An asphalt mixture normally has an internal friction angle between 20 and 60 degrees; thus, α ranges from 0.15 to 0.47 according to Equation 19. Therefore, the value of α is always greater than the value of β for an asphalt mixture, which means that a non-associated flow rule is applied to the asphalt mixture.

Evolution of Viscofracture

The evolution of viscofracture provides the changes of the anisotropic damage density with the variation of the stress. A pseudo J-integral Paris' law in terms of damage density is used to characterize the evolution of the viscofracture for the asphalt mixtures. The model is expressed as:

14

$$\frac{d\xi_i}{dN} = A_i \left(J_{Ri} \right)^{n_i} \qquad i = 1, 2 \tag{28}$$

where $i = 1, 2$ and $i = 1$ stands for the axial variable and $i = 2$ stands for the radial variable; ξ_i is the anisotropic damage density; A_i and n_i are coefficients of the Paris' law and are material constants, where A_i indicates the initial evolution speed of the viscofracture in terms of damage density and n_i indicates the increasing rate of the damage density evolution speed; and J_{Ri} is the pseudo J-integral that is interpreted as the dissipated energy for the growth of a unit crack surface area in the viscoelastic material. The pseudo J-integral can be calculated as:

$$J_{Ri} = \begin{cases} \int_0^t D(t-s) \dfrac{\partial K^2}{\partial s} ds \ \ or \\[2ex] \dfrac{\partial DPFSE^A}{\partial (c.s.a.)_i} \end{cases} \tag{29}$$

where $D(t)$ is the creep compliance; s is the current time before time t; K is the stress intensity factor under a repeated load; $DPFSE^A$ is the apparent dissipated pseudo fracture strain energy that can be computed by integrating stress over viscofracture strain; and $(c.s.a.)_i$ is the crack surface area projected on a specific direction and is determined as two times the projected lost area on the specific direction.

3. LABORATORY EXPERIMENTS AND MATERIAL PROPERTY CHARACTERIZATIONS

The systemic testing protocol employed in this study to determine the model parameters and the material properties is described in this chapter. The data analysis methods used to accurately perform the anisotropic, viscoelastic, viscoplastic, and viscofracture characterizations of asphalt mixtures are also presented.

Laboratory Experiments

Testing Materials

Twenty-four lab-mixed-lab-compacted (LMLC) asphalt mixture specimens were fabricated with the following variables:

- Two types of asphalt binders were fabricated: Asphalt V (PG 64-16) and Asphalt N (PG 76-22).

- Two air void contents were used: 4 percent and 7 percent (variation within ±0.5 percent).

- Three aging periods—0 months, 3 months, and 6 months—were continuously aged at 60°C.

- Two replicate specimens were fabricated for each combination of asphalt binder, air void content, and aging period.

A commonly used Texas limestone labeled Hanson limestone, shipped from New Braunfels, Texas, was selected for this study. The gradation of the aggregates was determined based on a Type C dense gradation specified by the Texas Department of Transportation (TxDOT; 2004). The optimum asphalt content was calculated based on the TxDOT test procedure (TxDOT, 2008) and was determined as 4.4 percent for the two binders (i.e., NuStar and Valero). In this report, VHL stands for the asphalt mixtures using the Valero binder and the Hanson limestone, and NHL stands for the asphalt mixtures using the NuStar binder and the Hanson limestone. The asphalt mixtures were compacted using a Superpave gyratory compactor for cylindrical samples with 150 mm in diameter and 175 mm in height. Then, the samples were cored to 100 mm in diameter and were cut to 150 mm in height.

Testing Protocols

The existing constitutive characterization of asphalt mixtures normally has a limitation in its model parameter determination. The test methods are complicated, time consuming, and costly when determining model parameters. The operations of the tests sometimes require expensive and complex apparatus. This study overcame the above shortcomings and developed proposed testing methods that are simple, fast, and accurate and can be performed by affordable and accessible testing equipment.

The material properties of asphalt mixtures were separated into nondestructive properties, including viscoelastic properties and inherent anisotropy, and destructive properties, including viscoplastic and viscofracture properties. Table 1 summarizes the material properties, model parameters, physical meanings, and corresponding test methods. Five common test methods were used for determining the material properties and model parameters of asphalt mixtures:

- Lateral surface scanning (hot-dog) test.
- Nondestructive dynamic modulus test.
- Destructive dynamic modulus test.
- Uniaxial compressive strength test.
- Triaxial compressive strength test.

The testing parameters, such as loading levels, loading rates, and testing temperatures, are summarized in Table 2. All of the tests in the testing protocol were conducted using the Universal Testing Machine (UTM). Before the tests, the asphalt mixture specimens were stored in an environmental chamber at the testing temperature for at least 3 h to reach the equilibrium temperature. The nondestructive creep test was first conducted, in which the total strain at the end of the test was controlled at less than 150 με, which is the linear viscoelastic limit for the asphalt mixture in compression (Levenberg and Uzan, 2004). Then the load was removed and the specimen was at rest for 1 h. The 1-h rest period was used for the following purposes: (a) the viscoelastic strains produced in the nondestructive tests were fully recovered and would not affect the results of the following tests; and (b) the 1-h rest period was needed to compensate for the temperature loss due to opening the door of the UTM chamber during the setup and operation of the tests. After the 1-h rest period, the destructive dynamic modulus test was performed on the same undamaged specimen, and a higher load, as shown in Table 2, was applied to the specimen.

18

Table 1. Summary of Material Properties, Model Parameters, and Determination Testing Methods of Compressive Characterization of Asphalt Mixtures.

Material Properties		Material Parameters		Testing Methods	Data for Parameter Determination
		Symbol	Physical Meaning		
Non-destructive Properties	Viscoelasticity	$E(t)$, E_Y	Relaxation and Young's Modulus	Uniaxial Compressive Creep (UCC) Tests	Creep Strain
		α_T	Time-Temperature Shift Factor		
		$\|E^*\|$	Magnitude of Dynamic Modulus	Nondestructive Dynamic Modulus (NDM) Test	Dynamic Strain and Stress
		δ, φ_{II}	Phase Angle of Dynamic Modulus		
	Inherent Anisotropy	Δ'	Modified Vector Magnitude	Lateral Surface Scanning Tests	Aggregate Size, Area, Aspect Ratio
Destructive Properties	Viscoplastic Yield Surface	α, ϕ	Slope, Internal Friction Angle	Uniaxial and Triaxial Compressive Strength (UCS/TCS) Tests	Initial Yield Strength
		κ_0, C	Intercept, Cohesion		
		d	Yield Extension Ratio		
	Strain Hardening Function	κ_1	Strain Hardening Amplitude		Yield Stresses during Strain Hardening
		κ_2	Strain Hardening Rate		
	Viscoplastic Potential Function	β	Slope of Viscoplastic Potential	N/A	Δ'
	Temperature and Strain Rate Dependence	a_T, ΔE_T	Temperature Effect Factor	UCS at Different Temperatures	Ultimate Yield Strength
		$a_{\dot{\varepsilon}}$, κ_3	Strain Rate Effect Factor	Destructive Dynamic Modulus (DDM) Tests	Separated Viscoplastic Strain
	Perzyna's Viscoplasticity	Γ	Viscosity Parameter		
		N	Rate Parameter		
	Viscofracture Damage Density Function	ξ_{ij}	Anisotropic Damage Density		Separated Viscofracture Strain (in Tertiary Stage)
		A_i, n_i	Coefficients in Paris' Law		
		N_f	Flow Number		

Table 2. Summary of Test Materials and Parameters for Compressive Characterization of Asphalt Mixtures.

Materials Tested	Testing Protocol			Test Efficiency
	Tests	Loading	Temperature	
ARC VHL and NHL mixtures: Binder: Valero (PG 64-16) NuStar (PG 67-22) Air Void: 4% 7% Period of Aging at 60°C: 0 month 3 months 6 months	Lateral Surface Scanning Test	N/A	Room temperature	• 5 min • Hot-dog tester • Portable scanner
	Uniaxial Compressive Creep Test	150 kPa (at 10°C) 80 kPa (at 25°C) 40 kPa (at 40°C) 15 kPa (at 60°C)	10°C 25°C 40°C 60°C	• 10 min for each test • Temperature change needs 2 h • UTM or Material Testing System (MTS)
	Nondestructive Dynamic Modulus Test	0.1 Hz; 0.5 Hz 1 Hz; 5 Hz 10 Hz; 25 Hz		
	Uniaxial Compressive Strength Test	311 με/s	40°C 50°C 60°C	• 5 min for each test • Temperature change needs 2 h • UTM or MTS
	Triaxial Compressive Strength Test	311 με/s <u>Confining pressures:</u> 103 kPa (15 psi) 207 kPa (30 psi)	40°C	
	Destructive Dynamic Modulus Test	Sinusoidal load (600 kPa)	40°C	• 2 h • UTM or MTS

Figure 3 shows the testing configuration of the uniaxial test. In the uniaxial test, the total axial deformation was recorded with respect to time using three vertical linear variable differential transformers (LVDTs). The axial strain was determined by dividing the average axial deformation by the axial gauge length (i.e., 90 mm in this study). A radial LVDT was mounted on a bracelet that surrounded the specimen to record the change of the specimen's circumference. The radial strain was calculated as the ratio of the circumferential deformation to the original circumference of the specimen (i.e., 314.2 mm). The conditions at the ends of all the tested specimens were treated to produce identical and approximately idealized end conditions (i.e., axial load was applied with very little lateral constraint or friction). The treatments, as shown in Figure 3, included (a) two soft rubber membranes placed between the end caps and the

specimens; and (b) wax-based petroleum jelly placed between the rubber membranes and the end caps. With the help of these treatments, the asphalt mixture specimens were found to be able to deform freely in the radial direction at the ends of the cylindrical specimens. The tested specimens also showed that the end constraints were negligible, and a uniform radial deformation was produced along the height of the specimens.

Figure 3. Testing configuration of uniaxial test.

The triaxial compressive strength tests required a confining pressure that was controlled during the test. The confining pressure was provided by the rapid triaxial testing (RaTT) cell of the UTM, which is shown in Figure 4. In the RaTT cell, the confining pressure was supplied by constant compressed air, and the asphalt mixture specimen was wrapped by a cylindrical rubber. Two vertical LVDTs and two radial LVDTs were used to record the vertical and horizontal deformation of the samples.

Figure 4. Testing configuration of triaxial test.

Characterization of Material Properties of Undamaged Asphalt Mixtures

Anisotropic Characterization

The inherent anisotropy of asphalt concrete is caused by the preferentially oriented aggregates resulting from the compaction during pavement construction. It is quantified by the modified vector magnitude (Δ') that is defined in Equation 2. The authors used a fast and simple test—the lateral surface scanning test—to determine Δ'. In this test, a cylindrical specimen (100 mm in diameter and 150 mm in height) was laid horizontally on an automatic rotator that rotated the sample at a constant speed. The lateral surface of the sample was scanned by a portable digital scanner to obtain a lateral surface image, which was then analyzed to determine the aggregates' properties including the inclination angle, the area, and the aspect ratio of the aggregate cutting surface. These measurements were used to calculate the modified vector magnitude in Equation 2. More details about the test and the analysis can be found in Zhang et al. (2011).

The lateral surface scanning tests were adopted in this study and performed on asphalt concrete concrete specimens that had the same binder, air void contents, and aging periods as those
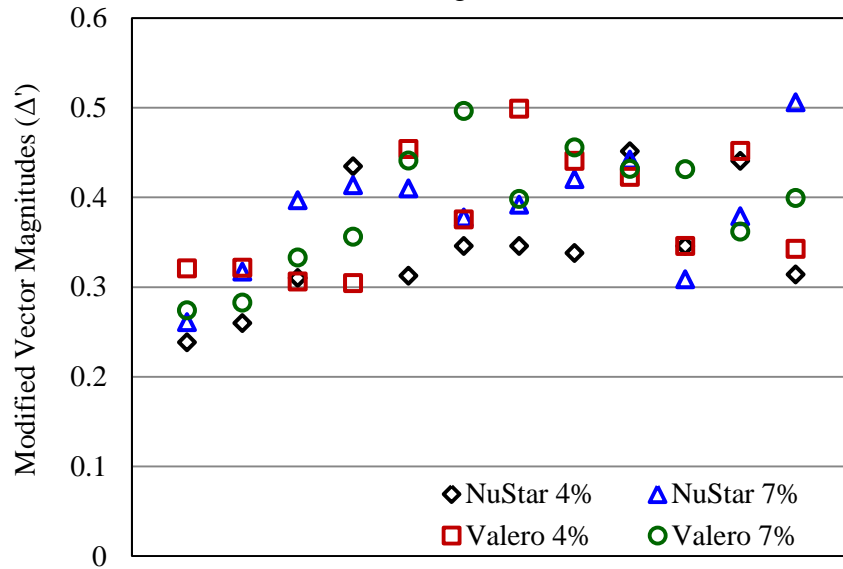
Figure 5 shows that the measured Δ' for the tested specimens and the values of Δ' varied from 0.2 to 0.5, which is consistent with the literature measurements (Zhang et al., 2011). However, no obvious relations were found between Δ' and the binder, air void content, and aging period. In fact, Δ' depends on the aggregate properties, including aggregate shape, size, and orientation, which are related to the aggregate gradation and the compaction effort during specimen fabrication.
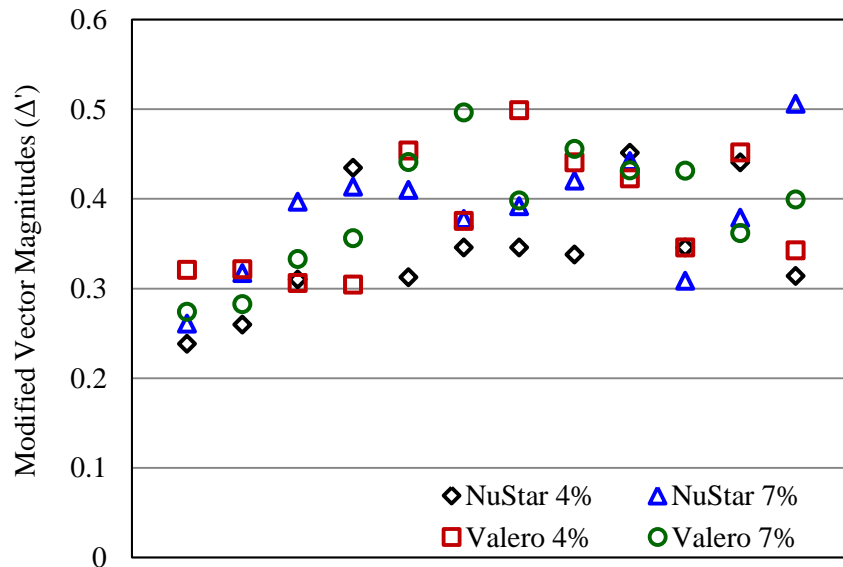
Figure 5. Measured modified vector magnitudes of asphalt concrete.

Viscoelastic Characterization

Creep Compliance and Relaxation Modulus

Based on the viscoelastic theories, the axial strain and stress can be related as follows:

$$\begin{cases} \varepsilon_1(t) = -\int_{0^-}^{t} D(t-\tau)d\sigma_1(\tau) \\ \sigma_1(t) = -\int_{0^-}^{t} E(t-\tau)d\varepsilon_1(\tau) \end{cases} \tag{30}$$

where $\varepsilon_1(t)$ is axial strain; $\sigma_1(t)$ is the applied stress that is a constant in the creep test; $D(t)$ is creep compliance; $E(t)$ is relaxation modulus; t is current time; and τ is a dummy variable that is less than or equal to t. Taking the Laplace transformation of Equation 30 gives a relationship between the creep compliance and the relaxation modulus:

$$\bar{E}(s)\bar{D}(s) = \frac{1}{s^2} \tag{31}$$

where $\bar{E}(s)$ and $\bar{D}(s)$ are the Laplace transforms of $E(t)$ and $D(t)$, respectively; and s is a variable in the Laplace domain.

The creep compliance and the relaxation modulus can be determined based on Equations 30 and 31 using the measured stress and strain in the compressive creep test. Then the creep compliance and the relaxation modulus are characterized using the Prony series model shown as follows:

$$D(t) = D_0 + \sum_{i=1}^{M} D_i \left[1 - \exp\left(-\frac{t}{\tau_i} \right) \right] \tag{32}$$

$$E(t) = E_\infty + \sum_{j=1}^{M} E_j \exp\left(-\frac{t}{k_j} \right) \tag{33}$$

where D_0 is instantaneous compliance; D_i represents components of creep compliance; τ_i is retardation time; E_∞ is the long-term equilibrium modulus; E_j represents the components of the relaxation modulus; k_j is the relaxation time; and M is the total number of Kelvin elements in the Prony series model. Young's modulus (E_Y) represents the instantaneous responses of the material and is determined as the initial relaxation modulus (i.e., $E_Y = E(t=0)$). More details can be found in the authors' previous study (Zhang et al., 2012b). An example test result is provided in Figure 6 to show the time-dependent creep compliance and relaxation modulus.
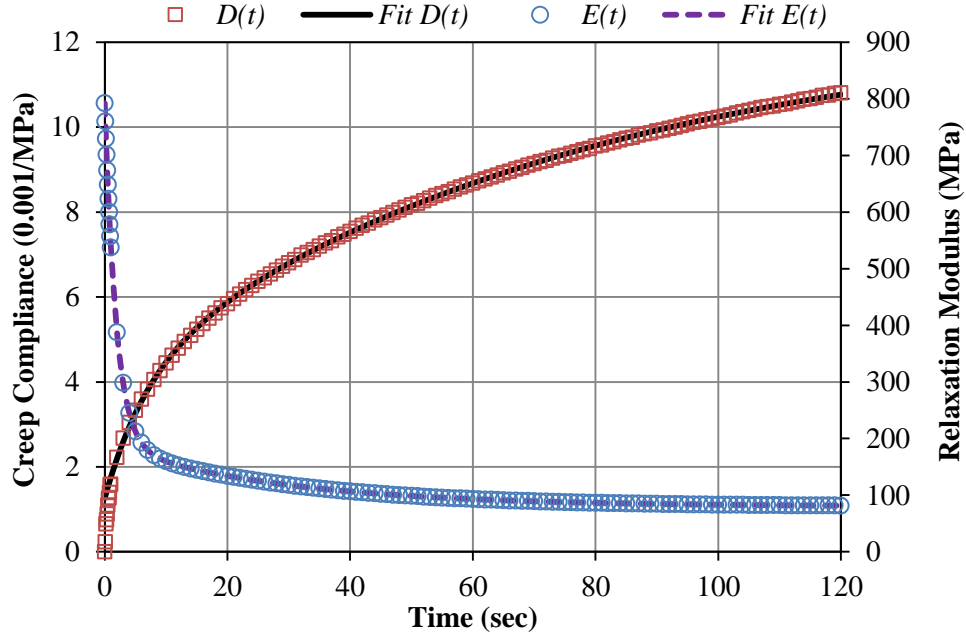
Figure 6. Creep compliance and relaxation modulus of an undamaged asphalt mixture at 40°C.

<u>Viscoelastic Poisson's Ratio and Viscoelastic Pi-son's Ratio</u>

Poisson's ratio ($\upsilon_{12}(t)$) is also an important material property that is a viscoelastic variable for an asphalt mixture. For the purpose of radial strain decomposition, another viscoelastic variable that is named as the Pi-son's ratio ($\pi_{12}(t)$) is proposed in this report. The viscoelastic Poisson's ratio and Pi-son's ratio are defined as:

$$\begin{cases} \varepsilon_2(t) = -\int_{0^-}^{t} \upsilon_{12}(t-s)d\varepsilon_1(s) \\ \varepsilon_1(t) = -\int_{0^-}^{t} \pi_{12}(t-s)d\varepsilon_2(s) \end{cases} \tag{34}$$

where $\upsilon_{12}(t)$ is the viscoelastic Poisson's ratio; $\pi_{12}(t)$ is the viscoelastic Pi-son's ratio; $\varepsilon_1(t)$ is the axial strain; and $\varepsilon_2(t)$ is the radial strain. $\pi_{12}(t)$ is used to determine the axial strain provided the radial strain is given. Taking the Laplace transform of Equation 34 yields:

$$\begin{cases} \upsilon_{12}(t) = \mathcal{L}^{-1}\left\{ -\dfrac{\bar{\varepsilon}_2(s)}{s\bar{\varepsilon}_1(s)} \right\} \\ \pi_{12}(t) = \mathcal{L}^{-1}\left\{ -\dfrac{\bar{\varepsilon}_1(s)}{s\bar{\varepsilon}_2(s)} \right\} \end{cases} \tag{35}$$

where $\mathcal{L}^{-1}\{f\}$ stands for the inverse Laplace transform of the function f. Equation 35 further provides a relationship between $\upsilon_{12}(t)$ and $\pi_{12}(t)$, as shown in Equation 36 which is a companion formula of Equation 31.

$$\bar{\pi}_{12}(s)\bar{\upsilon}_{12}(s) = \frac{1}{s^2} \tag{36}$$

where $\bar{\upsilon}_{12}(s)$ and $\bar{\pi}_{12}(s)$ are the Laplace transforms of $\upsilon_{12}(t)$ and $\pi_{12}(t)$, respectively.

   With the aid of the measured axial and radial strain in the nondestructive compressive creep test, Equation 35 is employed to determine $\upsilon_{12}(t)$ and $\pi_{12}(t)$, which are shown in Figure 7 as an example. It can be seen that $\upsilon_{12}(t)$ increases with time, while $\pi_{12}(t)$ decreases with time. $\upsilon_{12}(t)$ can be greater than 0.5, which is due to the anisotropic viscoelasticity of the asphalt mixture (Zhang et al., 2012a). The inverse viscoelastic Poisson's ratio is a decreasing curve and is always greater than 1.

   Comparing Figure 7 to Figure 6 suggests the idea to model $\upsilon_{12}(t)$ and $\pi_{12}(t)$ using the Prony series model. The formulas of $\upsilon_{12}(t)$ and $\pi_{12}(t)$ are expressed in Equations 37 and 38, which are companions of Equations 32 and 33, respectively.

$$\upsilon_{12}(t) = \upsilon_0 + \sum_{i=1}^{M} \upsilon_i \left[1 - \exp\left(-\frac{t}{r_i}\right)\right] \tag{37}$$

$$\pi_{12}(t) = \pi_\infty + \sum_{j=1}^{M} \pi_j \exp\left(-\frac{t}{z_j}\right) \tag{38}$$

where M is the total number of the Kelvin elements in the Prony series model; and υ_0, υ_i, r_i, π_∞, π_j, and z_j are parameters in the Prony model. υ_0 is the elastic Poisson's ratio, which is assigned as the pseudo Poisson's ratio used in the radial strain decomposition (i.e., $\upsilon_{12}^R = \upsilon_0$) in later sections. It is found from Figure 7 that the Prony series model can properly fit the measured $\upsilon_{12}(t)$ and $\pi_{12}(t)$.
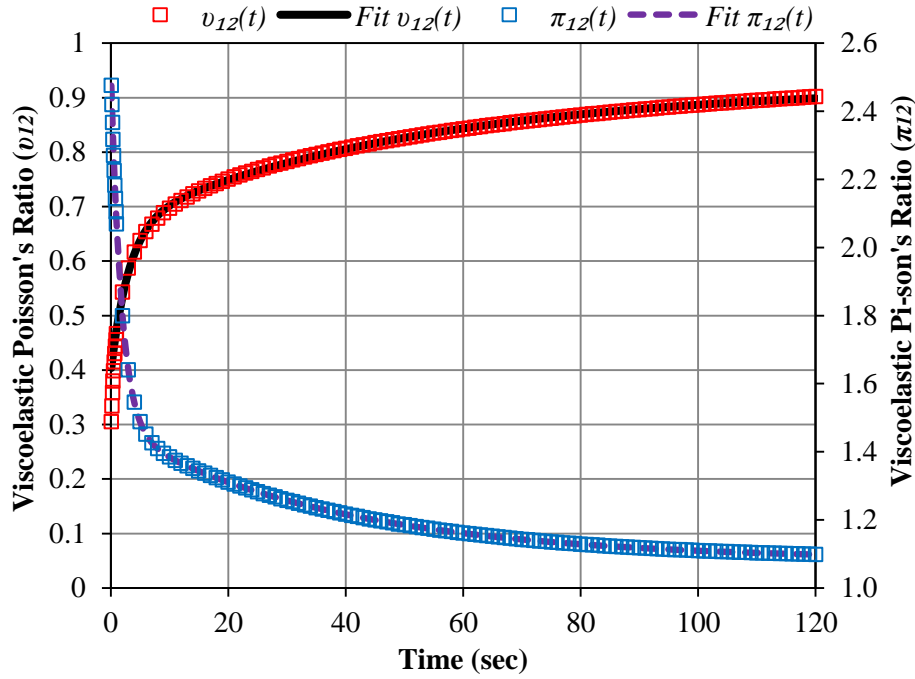
Figure 7. Viscoelastic Poisson's ratio and viscoelastic Pi-son's ratio of an undamaged asphalt mixture at 40°C.

Complex Modulus and Complex Poisson's Ratio

A complex variable has two components: magnitude and phase angle. The magnitude of the complex modulus is named as the dynamic modulus ($|E^*|$) in pavement engineering and is defined as the ratio of the amplitude of the oscillatory stress to the amplitude of the oscillatory strain. The phase angle (δ) of the complex modulus is determined as the time lag between the peak stress and the peak strain within one load cycle. The master curves of the dynamic modulus and phase angle have been discussed in the authors' previous work (Zhang et al., 2012a). The details of the determination of the dynamic modulus and phase angle can also be found in the literature (Zhang et al., 2012b). An example result of $|E^*|$ and δ is provided in Figure 8, which shows that $|E^*|$ and δ remain unchanged as the number of load cycles increases in the nondestructive compressive dynamic modulus test. This finding is also demonstrated by the testing results of the other 23 tested mixtures.
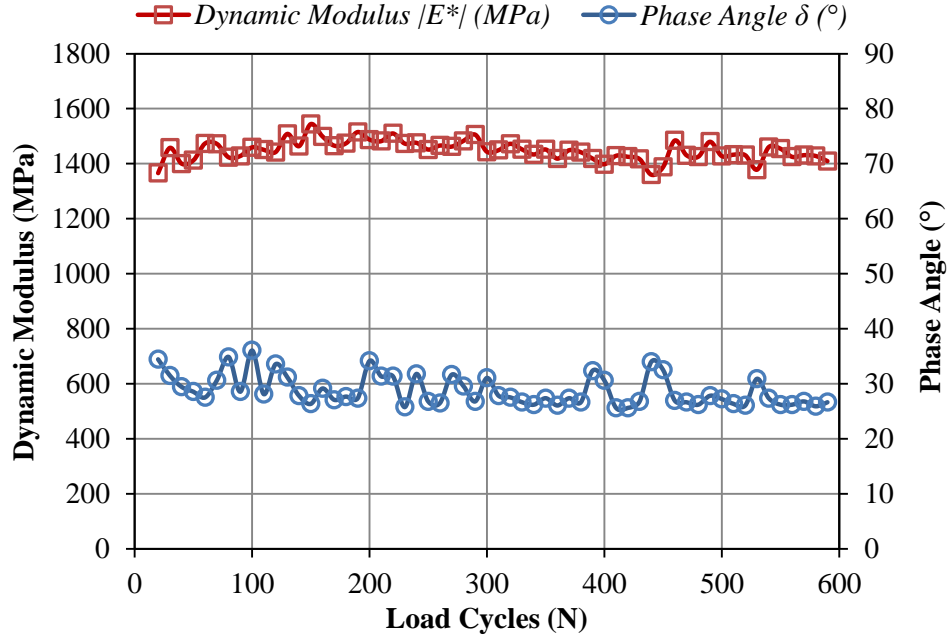
Figure 8. Dynamic modulus and phase angle of an undamaged asphalt mixture at 40°C and 1 Hz.

The complex Poisson's ratio (υ_{12}^*) is another critical material property when an asphalt mixture is subject to an oscillatory load. The magnitude of the complex Poisson's ratio ($\left|\upsilon_{12}^*\right|$) is defined as the amplitude ratio of the radial strain to the axial strain. The phase angle (δ') of the complex Poisson's ratio is determined as the time by which the peak radial strain lags behind the peak axial strain within one load cycle. Figure 9 shows $\left|\upsilon_{12}^*\right|$ and δ' as example asphalt mixtures and demonstrates that both $\left|\upsilon_{12}^*\right|$ and δ' are independent of time or load cycle in the nondestructive tests. This conclusion is verified by the testing results of the other 23 tested mixtures.

The average $\left|\upsilon_{12}^*\right|$ for the mixture shown in Figure 9 is determined as 0.34, which is less than 0.5. This is reasonable because the nondestructive dynamic modulus test is performed at 1 Hz, which corresponds to a creep time of 0.08 sec (i.e., creep time $t = 1/(2\zeta) = 1/(4\pi\omega) = 0.08$ sec, where ζ is frequency in rad/sec; and ω is frequency in Hz ($\omega = 1$ Hz in this study). In such a short loading time (i.e., 0.08 sec), the material behaves more elastically and the value of $\left|\upsilon_{12}^*\right|$ approximately equals $\upsilon_{12}(t = 0.08\,\text{sec})$, which is 0.34 according to the measurements in Figure 7.
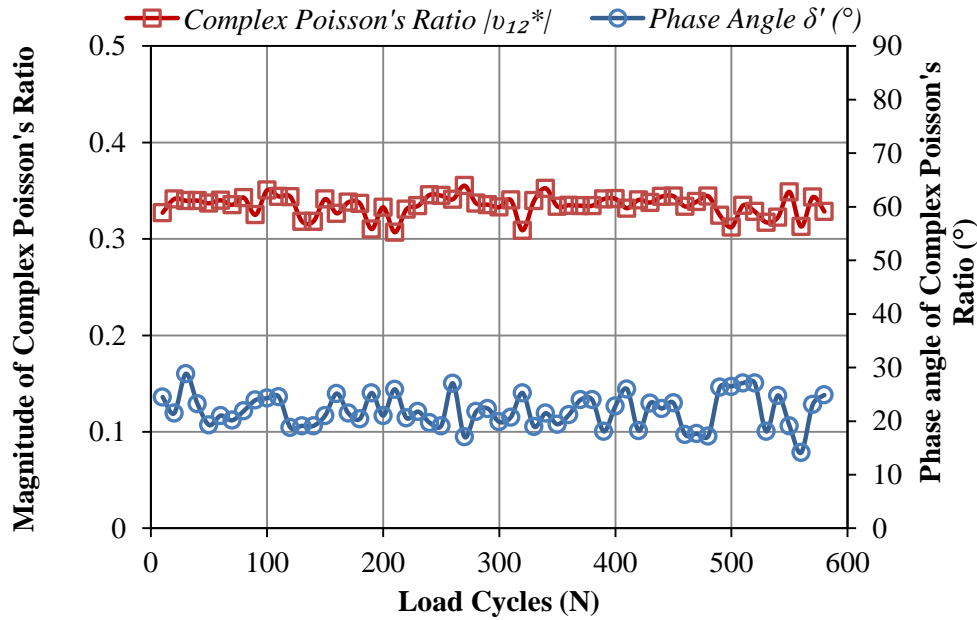
Figure 9. Magnitude and phase angle of complex Poisson's ratio of an undamaged asphalt mixture at 40°C and 1 Hz.

Characterization of Material Properties of Damaged Asphalt Mixtures

Yield Strength Characterization

The yielding strength properties include Young's modulus (E_Y), initial yield strength (σ_y) of the UCS test, yield surface slope (α), yield surface intercept (κ_0), cohesion (C), internal friction angle (ϕ), and extension ratio (d). To obtain these material properties, the initial yield strength (σ_y) should first be determined. σ_y is normally defined as the stress at which the plastic (or viscoplastic) deformation begins. For the elastoplastic material (e.g., metal), σ_y is determined as the separation point at which the stress-strain curve of a strength test transits from the linear part (elastic domain) to the nonlinear part (plastic domain). However, for a viscoplastic material like asphalt concrete, no linear part can be observed on the stress-strain curve measured in the strength test. As shown in Figure 10, the stress-strain curve shows a nonlinear relationship even at a very small load level, and no obvious separation point can be identified on the stress-strain curve. Based on this observation, some researchers (Drescher et al., 1993; Lu and Wright, 1998) concluded that no yielding threshold (i.e., σ_y) exists for asphalt concrete.

29
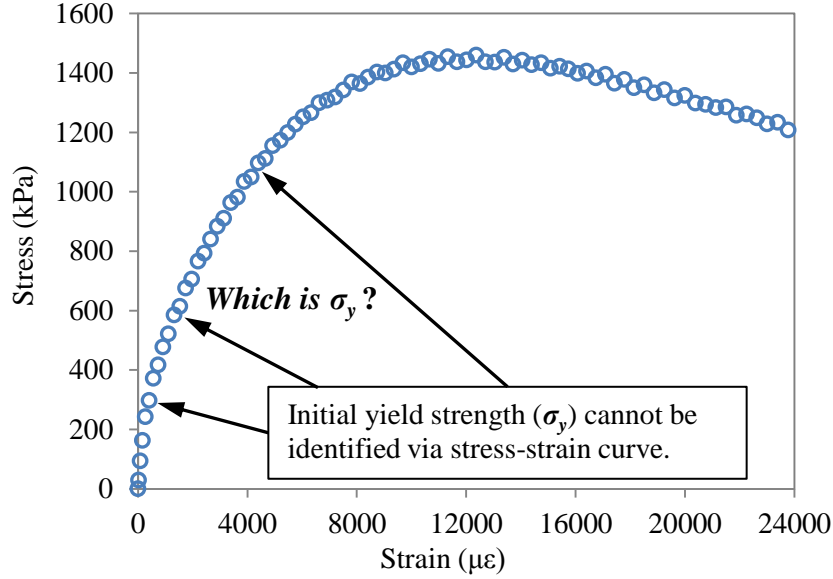
Figure 10. Typical stress-strain curve in a uniaxial compressive strength test of an asphalt mixture at 40°C and 311 µε/s.

In fact, the nonlinearity of the stress-strain curve is caused by the relaxation of the viscoelastic material, which can be explained by a simple mechanistic analysis: if the input of the strength test is a controlled strain ($\varepsilon = ct$ where c is the constant strain rate), the output stress of the strength test in the viscoelastic field (before the yielding threshold) is theoretically calculated as $\sigma = c \int_0^t E(s)ds$. The strain is linear with time, while the stress is nonlinear with time; thus, the stress is nonlinearly related to the strain, and the stress-strain curve becomes nonlinear even in the viscoelastic domain. Because of the nonlinearity of the stress-strain curve, the traditional approach of determining the initial yield strength may not apply to asphalt concrete.

However, asphalt concrete does have a yielding threshold that separates the viscoelastic part from the viscoplastic part of the stress-strain curve. An analytical method using the pseudostrain concept is proposed in this report to effectively and accurately determine the initial yield strength of the asphalt concrete, as illustrated by the following steps.

First, the relaxation modulus is determined from the UCC tests and modeled by the Prony series model, as in Equation 33. Second, the pseudostrain in a strength test is calculated based on its definition as follows (Schapery, 1984):

$$\varepsilon^R(t) = \frac{1}{E_R} \int_0^t E(t-s) \frac{d\varepsilon(s)}{ds} ds = \frac{c}{E_R} \left[E_\infty t + \sum_{j=1}^M E_j k_j \left(1 - e^{-\frac{t}{k_j}} \right) \right] \tag{39}$$

30

where c is the constant strain rate; and E_R is the reference modulus, which is assigned to be equal to the Young's modulus of the asphalt concrete ($E_Y = E(t = 0)$)) and represents the elastic/ instantaneous responses of the viscoelastic materials.

Third, the measured stress is plotted against the pseudostrain, as shown in Figure 11, which has a linear portion ($R^2 = 0.9989$) with a slope of Young's modulus. The initial data (before the linear portion) in Figure 11 showing nonlinearity is caused by the machine compliance in the crosshead strain control mode. The initial yield strength (σ_y) is determined as the stress at the end of the linear portion on the stress-pseudostrain curve. The σ_y determined from uniaxial and triaxial strength tests is employed to calculate the material properties, such as C, ϕ, α, and κ_0.
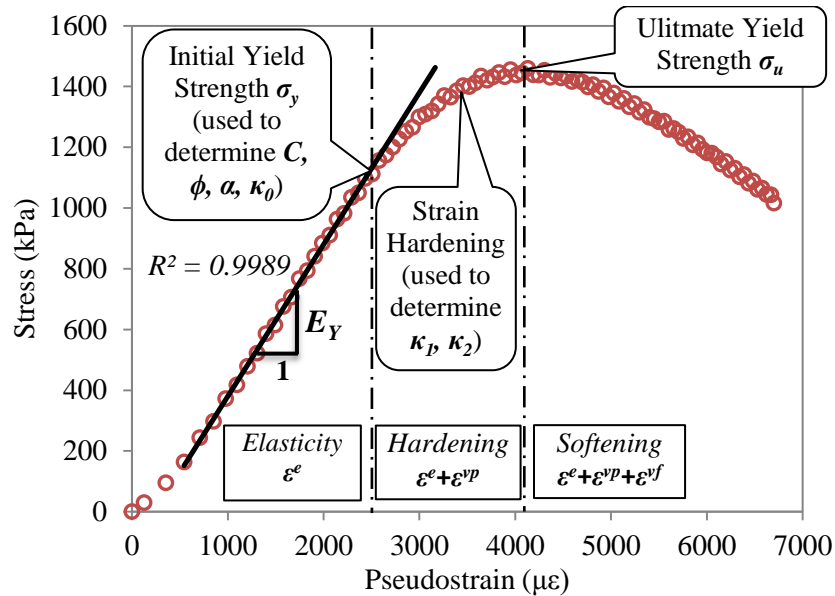
Figure 11. Stress versus pseudostrain in a uniaxial compressive strength test of an asphalt concrete at 40°C and 311 με/s.

The reason for using the pseudostrain rather than total strain is that when E_R is equal to the Young's modulus, the pseudostrain is demonstrated to be equal to the remaining strain after subtracting the viscous strain (ε^{vi}) from the total strain (ε^{T}) (Zhang et al., 2012b). In other words, the pseudostrain is the strain component after removing the viscous effect on the material responses. Before yielding occurs, the pseudostrain shows a linear relation with stress since it is equivalent to the elastic strain (ε^{e}). As viscoplastic deformation occurs, the pseudostrain is equal to the sum of ε^{e} and viscoplastic strain (ε^{vp}). The stress-pseudostrain curve from the initial yield

strength (σ_y) to the ultimate yield strength (peak stress, σ_u) shows a nonlinear relation, as shown in Figure 11, which actually is the strain hardening process. The determinations of the hardening parameters (i.e., κ_1 and κ_2) are based on this portion of the curve. According to the above analysis, a strain decomposition can be performed on the total strain before σ_u in the strength test:

$$\begin{cases} \varepsilon^e = \sigma/E_Y \\ \varepsilon^{vi} = \varepsilon^T - \varepsilon^R \\ \varepsilon^{vp} = \varepsilon^R - \varepsilon^e \end{cases} \tag{40}$$

The slope (α) and intercept (κ_0) of the proposed GD-P yield surface model were calculated based on σ_y determined in the UCS and TCS tests. At the reference temperature and strain rate, Equation 15 gives the initial yield surface function as follows:

$$\frac{\sigma_y - p}{\sqrt{3}} - \alpha\left(\sigma_y + 2p\right) - \kappa_0 = 0 \tag{41}$$

where p is the confining pressure. Using the data of σ_y at three different confining pressures ($p = 0, 103, 207 \, \text{kPa}$), α and κ_0 were determined for all of the tested asphalt concretes and are shown in the next chapter.

The cohesion (C) and internal friction angle (ϕ) for the asphalt concretes were also determined based on the UCS and TCS testing results. The Mohr-Coulomb initial yield surface function is written as:

$$\frac{\sigma_y - p}{2} = \frac{\sigma_y + p}{2}\sin\phi - C\cdot\cos\phi \tag{42}$$

Employing the data of σ_y at different p values, C and ϕ were determined and are also shown in the next chapter.

Strain Hardening Characterization

At the reference temperature and strain rate, the GD-P model gives the hardening yielding surface functions in uniaxial condition as follows:

$$\frac{\sigma_1}{\sqrt{3}} - \alpha\sigma_1 - \kappa_0 = \kappa_1\left[1 - \exp\left(-\kappa_2\varepsilon_e^{vp}\right)\right] \tag{43}$$

where σ_1 is the measured stress during strain hardening that is the stress between σ_y and σ_u;

and $\varepsilon_e^{vp} = \varepsilon_1^{vp}$, which is the axial viscoplastic strain of the UCS test and is calculated as

$\varepsilon_1^{vp} = \varepsilon^R - \sigma_1/E_Y$ based on Equation 40. Figure 12 shows an example of the $\sigma_1 \sim \varepsilon_e^{vp}$ curve.
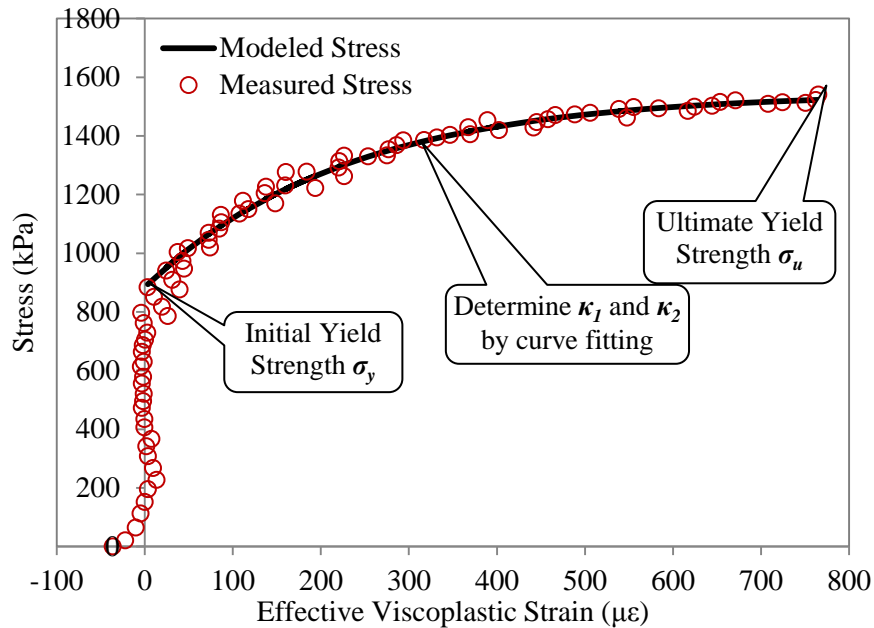
Figure 12. Stress versus effective viscoplastic strain in a uniaxial compressive strength test of an asphalt concrete at 40°C.

As Figure 12 illustrates, ε_e^{vp} does not occur before σ_y, and the stresses show an increasing power curve with ε_e^{vp} during strain hardening. The measured $\sigma_1 \sim \varepsilon_e^{vp}$ data are modeled by the exponential function shown in Equation 21. The modeled stresses are plotted as the solid curve in Figure 12, and the hardening parameters κ_1 and κ_2 are determined by fitting Equation 21 to the $\sigma_1 \sim \varepsilon_e^{vp}$ data. One can conclude that the strain hardening model using an exponential function can perfectly model the measured stresses during strain hardening in the strength tests. The same data analyses were performed on all of the tested asphalt concretes, and the determined κ_1 and κ_2 for different asphalt concretes are shown and discussed in the next chapter.

Temperature Effect on Viscoplastic Yielding

The UCS tests were performed on the asphalt mixture specimens at five different temperatures (40°C, 45°C, 50°C, 55°C, and 60°C). Figure 13 shows the measured stress-strain curves at the five temperatures. Each curve is an average of the testing data from two replicate

specimens. As the figure shows, the yield strength decreases as the temperature increases, which is due to the lower cohesion of the asphalt concrete at a higher temperature. One can easily determine the ultimate yield strengths (σ_u), which are peak stresses of the stress-strain curves and are shown in Figure 13.

The figure plots Stress (kPa) versus Strain (με) with curves labeled 40°C, 45°C, 50°C, 55°C, 60°C, and includes the following data table:

Temperatures		σ_u	a_T	
°C	K	kPa	Calculated	Modeled
40	313.15	2224	1.02	1.00
45	318.15	2094	0.96	0.88
50	323.15	1746	0.80	0.78
55	328.15	1609	0.74	0.69
60	333.15	1199	0.55	0.62
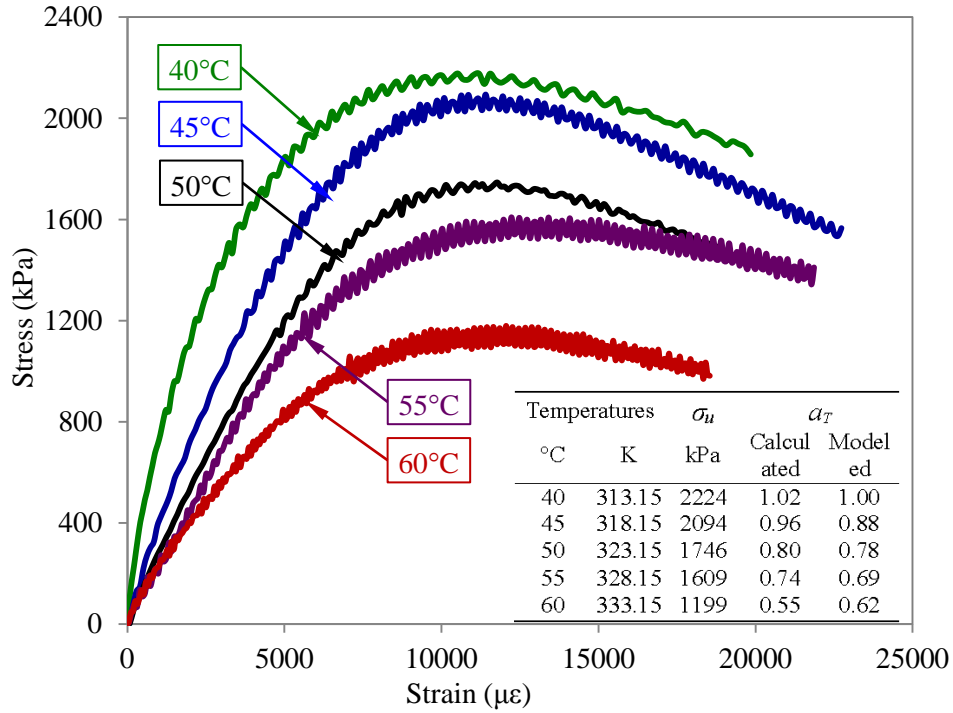
Figure 13. Measured stress versus strain in uniaxial strength tests of asphalt concretes at different temperatures and the data of ultimate yield strengths (σ_u) and temperature factors (a_T).

The values of σ_u determined from stress-strain curves were employed to calculate a_T. At the moment of σ_u, the strain hardening becomes saturated and the yield surface function in the uniaxial condition is:

$$\frac{\sigma_u}{\sqrt{3}} - \alpha\sigma_u = \left(\kappa_0 + \kappa_1\right)a_T \tag{44}$$

where α, κ_0 and κ_1 are yielding parameters determined at the reference temperature (i.e., 40°C in this study). Thus, the values of a_T were solved based on Equation 44 and are shown in Figure 13. The relationship between a_T and temperature (in Kelvin) was also modeled by the Arrhenius model in Equation 22. Using the measured data of a_T, the activation energy for the temperature

effect (ΔE_T) was determined to be 21,020 J/mol for this asphalt concrete, and values of the modeled a_T are shown in Figure 13. The decreasing a_T with temperature quantifies the loss of the cohesion and strain hardening amplitude due to the increasing temperature.

Strain Rate Effect on Viscoplastic Yielding

The UCS tests were also performed on the asphalt mixture specimens at 40°C using five different strain rates (i.e., 18 με/sec, 65 με/sec, 311 με/sec, 622 με/sec, and 1,074 με/sec). Figure 14 illustrates the stress-strain curves of the UCS tests at the five strain rates. Each curve is an average of the testing data from two replicate specimens. As shown in Figure 14, the yield stress increases with the increasing strain rate, which indicates that a larger cohesion and the strain hardening amplitude are obtained for the asphalt concrete at a higher strain rate. To determine $a_{\dot{\varepsilon}}$, σ_u was acquired from the stress-strain curves, and Figure 14 shows that σ_u increases with an increase of the strain rate.

At a constant temperature, $a_T = 1$ and the yield surface function at σ_u of the UCS tests is:

$$\frac{\sigma_u}{\sqrt{3}} - \alpha\sigma_u = \left(\kappa_0 + \kappa_1\right)a_{\dot{\varepsilon}} \tag{45}$$

where α, κ_0, and κ_1 are yielding parameters determined at the reference strain rate (i.e., 311 με/sec in this study). By substituting σ_u in Equation 45, the values of $a_{\dot{\varepsilon}}$ were resolved at the five different strain rates, which are shown as the calculated $a_{\dot{\varepsilon}}$ in Figure 14. The calculated values of $a_{\dot{\varepsilon}}$ were also modeled by the power function in Equation 23, in which the power coefficient κ_3 was determined as 0.196 for this asphalt mixture. The increasing $a_{\dot{\varepsilon}}$ following a power function with strain rates quantifies the effect of strain rate on the material cohesion and strain hardening during the viscoplastic deformation of asphalt concrete.

Strain rates	σ_u	$a_{\dot\varepsilon}$	
μɛ/sec	kPa	Calculated	Modeled
18	1123	0.56	0.57
65	1432	0.72	0.74
311	2021	1.01	1.00
622	2324	1.17	1.15
1074	2474	1.24	1.27
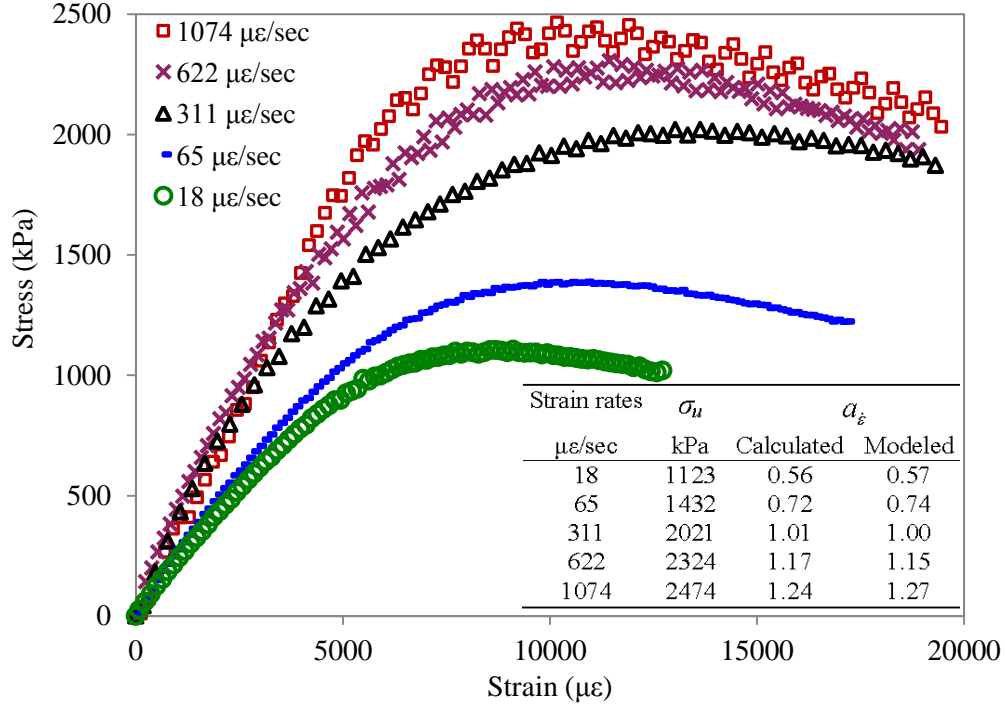
Figure 14. Measured stress versus strain in uniaxial strength tests of asphalt concretes at different strain rates and data of ultimate yield strengths (σ_u) and strain rate factors ($a_{\dot\varepsilon}$).

Viscofracture Characterization

The viscofracture properties of asphalt mixtures are represented by the material properties in the evolution equation that is the pseudo J-integral Paris' law in Equation 28. The pseudo J-integral can be calculated as:

$$J_{Ri} = \frac{\partial DPFSE^A}{\partial (c.s.a.)_i} = \frac{\partial DPFSE^A / \partial N}{\partial (c.s.a.)_i / \partial N} = \frac{\partial \left[\sigma_0^A \varepsilon_1^{vf}(N) \right] / \partial N}{\partial \left[2A_i^T \xi_i(N) \right] / \partial N} \tag{46}$$

where $(c.s.a.)_i$ is the crack surface area projected on a specific direction and $(c.s.a.)_i$ is determined as two times the projected lost area on the specific direction; and A_i^T is the total (apparent) area of the cross section. Substituting Equation 46 into Equation 28 and integrating both sides of Equation 28 yields:

$$\xi_i(N) = \xi_{0i} + (A_i)^{\frac{1}{1+n_i}} \left(\frac{\theta_1 \sigma_0^A \varepsilon_0^{vf}}{2A_i^T} \right)^{\frac{n_i}{1+n_i}} \left(\frac{1+n_i}{\theta_1 n_i} \right) \left[e^{\frac{\theta_1 n_i}{1+n_i}(N - N_f)} - 1 \right] \tag{47}$$

where ξ_{0i} is the damage density at the flow number. If making the following arrangement:

$$\begin{cases} C_i = \left(A_i\right)^{\frac{1}{1+n_i}} \left(\dfrac{\theta_1 \sigma_0^A \varepsilon_0^{vf}}{2A_i^T} \right)^{\frac{n_i}{1+n_i}} \left(\dfrac{1+n_i}{\theta_1 n_i} \right) \\ D_i = \dfrac{\theta_1 n_i}{1+n_i} \end{cases} \tag{48}$$

Equation 47 becomes:

$$\xi_i(N) = \xi_{0i} + C_i \left[e^{D_i\left(N-N_f\right)} - 1 \right] \tag{49}$$

Fitting Equation 48 to the axial and radial damage density curves determined by Equation 10 and 11, respectively, the parameters (C_i and D_i) can be obtained. Then, the material constants in Paris' law are determined as follows:

$$\begin{cases} A_i = \left(\dfrac{2A_0^T}{\theta_1 \sigma_0^A \varepsilon_0^{vf}} \right)^{n_i} \left(C_i D_i\right)^{1+n_i} \\ n_i = \dfrac{D_i}{\theta_1 - D_i} \end{cases} \tag{50}$$

Figure 15 and Figure 16 show the axial and radial damage densities for an asphalt mixture with a 4 percent air void content and an asphalt mixture with a 7 percent air void content, respectively. It can be concluded that the asphalt mixture with 4 percent air void content has a higher radial damage density and a lower axial damage density, while the asphalt mixture with 7 percent air void content has a lower radial damage density and a higher axial damage density. The same conclusion can be made for all of the tested asphalt mixtures that include two binders, two air void contents, and three aging periods.

Results of the material constants in Paris' law for different asphalt mixtures are determined by Equation 50 and presented and discussed in the next chapter.
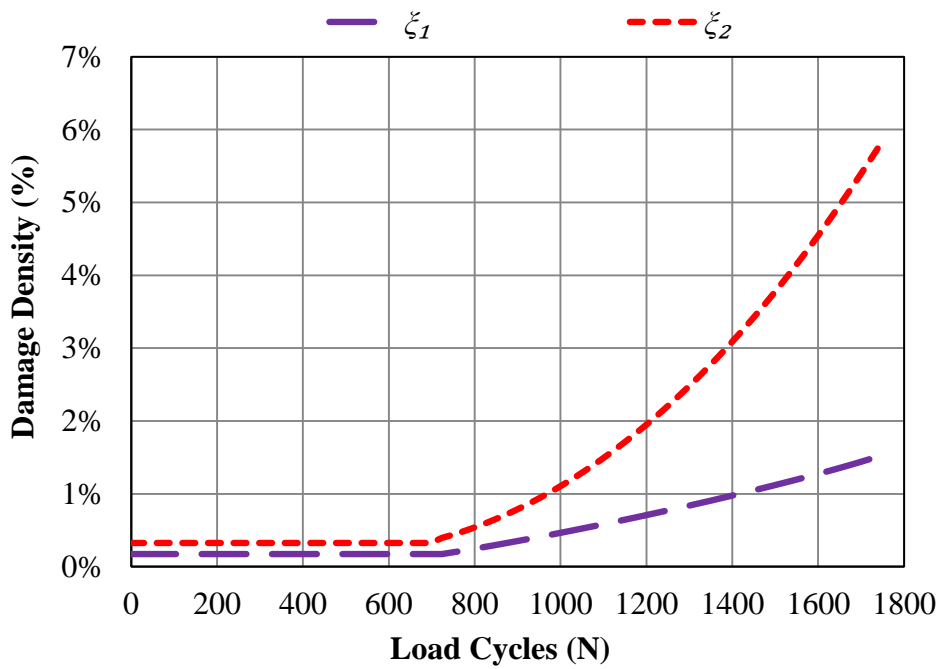
Figure 15. Axial and radial damage densities for an asphalt mixture with 4 percent air voids.
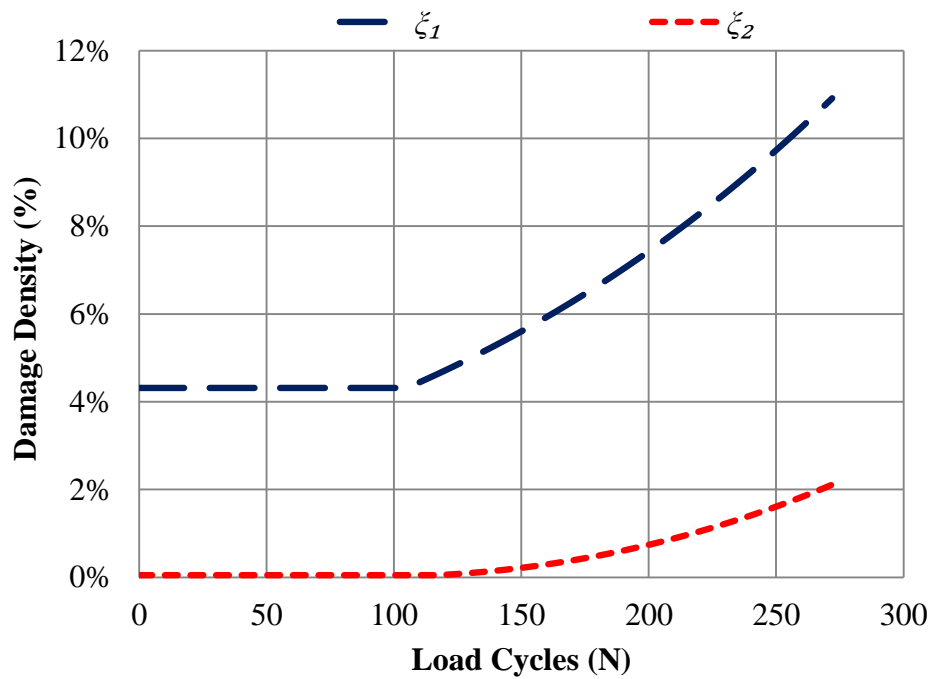
Figure 16. Axial and radial damage densities for an asphalt mixture with 7 percent air voids.

4. EXPERIMENTAL RESULTS AND MODEL VALIDATIONS

Testing results including the material properties and model parameters are presented and discussed in this chapter for the asphalt mixtures with different binders, air void contents, and aging periods. Additional laboratory tests other than the tests that were used to determine the model parameters were performed to validate the proposed viscoplastic models.

Testing Results and Discussions

Summary of Testing Results

The measured results for the material properties and viscoplastic model parameters of the tested asphalt mixtures that had two different binders (i.e., Binder N: PG 64-16; and Binder V: PG 76-22), two air void contents (i.e., 4 percent and 7 percent), and three aging periods (i.e., unaged, 3-month, and 6-month continuous aging at 60°C) were collected and are summarized in Table 3 and Table 4. Table 3 shows the measured results of the inherent anisotropy, viscoelasticity, and viscofracture properties of the asphalt mixtures, and Table 4 shows the measured results of the viscoplasticity properties of the asphalt mixtures. In the tables, VHL stands for the asphalt mixtures using Binder V and the Hanson limestone. NHL stands for the asphalt mixtures using Binder N and the Hanson limestone.

Table 3. Measured Results of the Inherent Anisotropy, Viscoelasticity, and Viscofracture Properties for Different Asphalt Mixtures.

Material Properties			Inherent Anisotropy	Viscoelasticity				Viscofracture				
			Modified Vector Magnitude	Young's Modulus	Dynamic Moudlus	Phase Angle	Phase Angle in Phase II	Flow Number	Paris' Law's Coefficients for Axial Damage		Paris' Law's Coefficients for Radial Damage	
Physical Meaning												
Asphalt Mixtures			Δ'	E_Y	$|E^*|$	δ	φ_{II}	Nf	A_1	n_1	A_2	n_2
Binder	Air Void	Aging Months	N/A	MPa	MPa	degrees	degrees	cycles	1/cycle	N/A	1/cycle	N/A
NHL PG64-16	4%	0	0.3106	656	1513	31.7	20.4	824	3.04E-14	1.369	1.75E-10	1.115
		3	0.3354	1108	2015	28.9	20.3	1153	3.19E-16	1.731	7.05E-14	2.555
		6	0.3880	1670	3435	26.5	21.6	3156	3.79E-20	1.965	1.75E-23	4.593
	7%	0	0.3471	455	502	33.1	21.4	37	1.90E-10	1.265	2.02E-05	0.000
		3	0.3998	906	1438	30.2	24.1	435	2.71E-13	1.502	8.12E-07	0.419
		6	0.4088	1352	2072	28.5	21.2	1718	1.42E-17	1.688	2.21E-09	1.100
VHL PG76-22	4%	0	0.3131	759	1531	36.8	25.1	282	1.44E-08	0.602	1.71E-07	0.657
		3	0.4422	1354	3093	32.1	23.3	1050	6.18E-11	0.843	3.88E-12	1.409
		6	0.3907	1575	3268	30.6	24.2	1650	2.02E-12	0.956	2.22E-16	1.963
	7%	0	0.3114	540	998	36.7	20.3	119	1.23E-06	0.486	1.39E-05	0.071
		3	0.4478	1019	2181	34.4	23.9	375	6.99E-10	0.782	4.10E-17	2.107
		6	0.4060	1099	2407	32.2	24.7	713	1.87E-10	0.839	2.01E-19	2.464

Table 4. Measured Results of Viscoplasticity Properties for Different Asphalt Mixtures.

Material Properties			Viscoplasticity												
Physical Meaning			Perzyna's Coefficients		Initial Yield Strength	Cohesion	Internal Friction Angle	Slope of Yield Surface	Intercept of Yield Surface	Coefficients of Strain Hardening		Rate Coefficient	Extension Ratio	Slope of Plastic Potential
Asphalt Mixtures			Γ	N	σ_y	C	φ	α	κ_0	κ_1	κ_2	κ_3	d	β
Binder	Air Void	Aging Months	1/sec	N/A	kPa	kPa	Degrees	N/A	kPa	kPa	1/με	N/A	N/A	N/A
NHL PG64-16	4%	0	1.30E-07	1.71	675.3	143.6	46.8	0.370	150.8	75.0	0.0031	0.23	0.61	0.17
		3	9.12E-08	1.71	1194.4	227.3	48.9	0.382	241.5	111.0	0.0110	0.30	0.60	0.19
		6	2.31E-08	1.77	1486.9	302.5	45.9	0.363	319.6	148.6	0.0064	0.29	0.61	0.22
	7%	0	2.53E-07	1.59	566.0	119.8	43.0	0.340	131.0	72.0	0.0116	0.26	0.63	0.19
		3	1.52E-07	1.90	731.6	164.8	44.4	0.350	179.4	91.4	0.0093	0.31	0.62	0.22
		6	8.90E-08	1.90	990.1	203.9	44.8	0.354	218.4	107.8	0.0044	0.24	0.62	0.23
VHL PG76-22	4%	0	2.20E-07	1.82	835.3	191.9	43.1	0.339	211.7	75.9	0.0083	0.37	0.63	0.17
		3	8.23E-08	1.66	1451.2	307.6	45.0	0.351	339.9	152.5	0.0049	0.37	0.62	0.25
		6	4.55E-08	1.64	1560.6	328.1	45.7	0.361	349.4	154.9	0.0052	0.34	0.61	0.22
	7%	0	4.50E-07	2.10	419.1	93.9	44.1	0.349	101.5	63.9	0.0080	0.35	0.62	0.17
		3	1.32E-07	1.69	824.3	190.0	42.9	0.338	209.7	102.8	0.0066	0.32	0.63	0.25
		6	8.70E-08	1.79	1009.8	238.0	41.5	0.326	266.7	130.9	0.0035	0.35	0.64	0.23

Discussions of Material Properties of Asphalt Mixtures

Viscoelastic Material Properties of Different Asphalt Mixtures

Figure 17 shows the measured Young's moduli and the initial yield strengths in the UCS test for different asphalt mixtures at 40°C. It was found that both E_Y and σ_y increased as the air void content decreased or the aging period increased. No significant differences were found between the asphalt mixtures with different binders. A relationship was obtained, as shown in Equation 51, between the initial yield strength and the Young's modulus with an acceptable coefficient of determination (R^2).

$$\sigma_y\left(kPa\right)=0.8782\times E_Y\left(MPa\right)+64.32 \quad R^2=0.8306 \tag{51}$$

Equation 51 indicates that a stiffer asphalt mixture tends to have a higher initial yield strength. It must be emphasized that the relationship between E_Y and σ_y can be affected by loading rate, confinement, and temperature.

Figure 18 shows the dynamic modulus and phase angle for different asphalt mixtures. It was found that the dynamic modulus increased and the phase angle decreased when asphalt mixtures became stiffer, which may have been caused by a stiffer binder, a lower air void content, or a longer aging period. Table 3 indicates that the phase angle for the undamaged asphalt mixtures was always less than the phase angle in the secondary stage because the asphalt

mixtures were compressed and the air voids were squeezed during the primary stage. Thus, the material became stiffer, and the phase angle in the secondary stage turned out to be smaller than the initial value, which was the phase angle of the undamaged material.
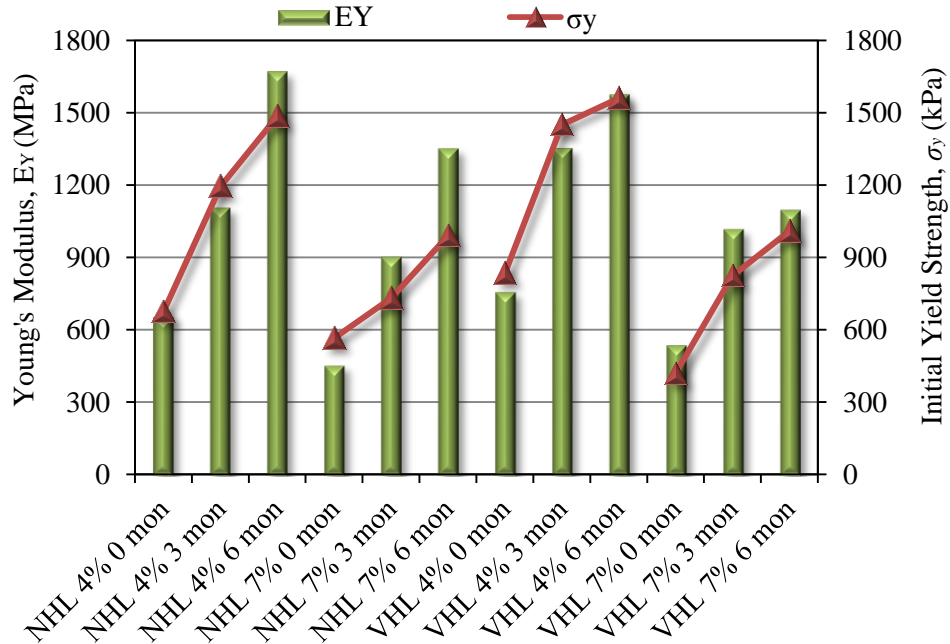
Figure 17. Young's modulus and initial yield strength in uniaxial compressive strength test for different asphalt mixtures at 40°C.
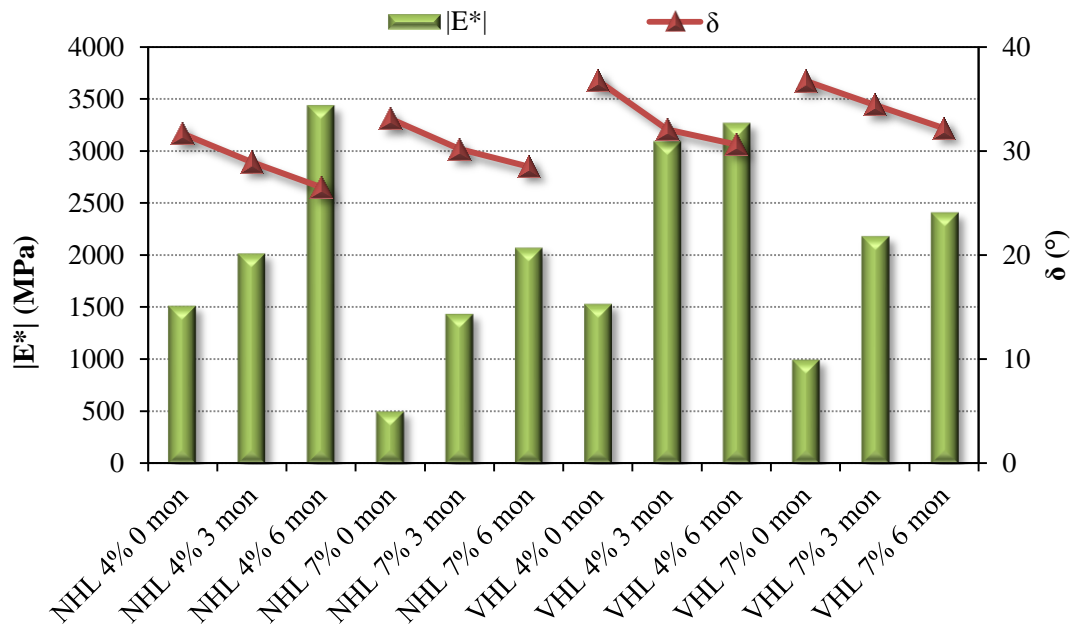
Figure 18. Dynamic modulus and phase angle for different asphalt mixtures at 40°C.

41

Viscoplastic Material Properties of Different Asphalt Mixtures

The slope (α) and intercept (κ_0) of the yield surface were determined for varieties of asphalt mixtures and are shown in Figure 19. The cohesion (C) and internal friction angle (ϕ) of the asphalt mixtures were determined and are shown in Figure 20.
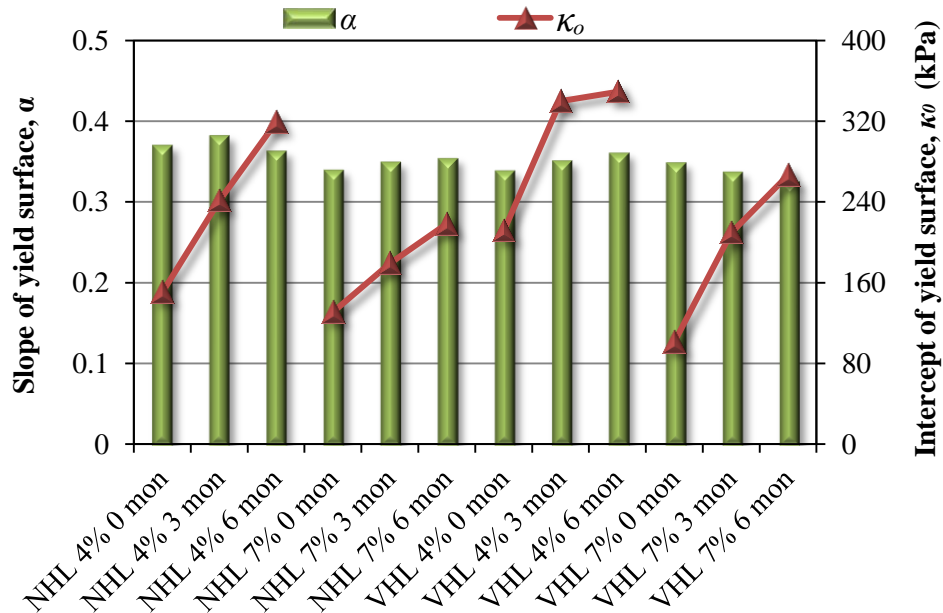
Figure 19. Slope and intercept of the GD-P yield surface on meridian plane for different asphalt mixtures.
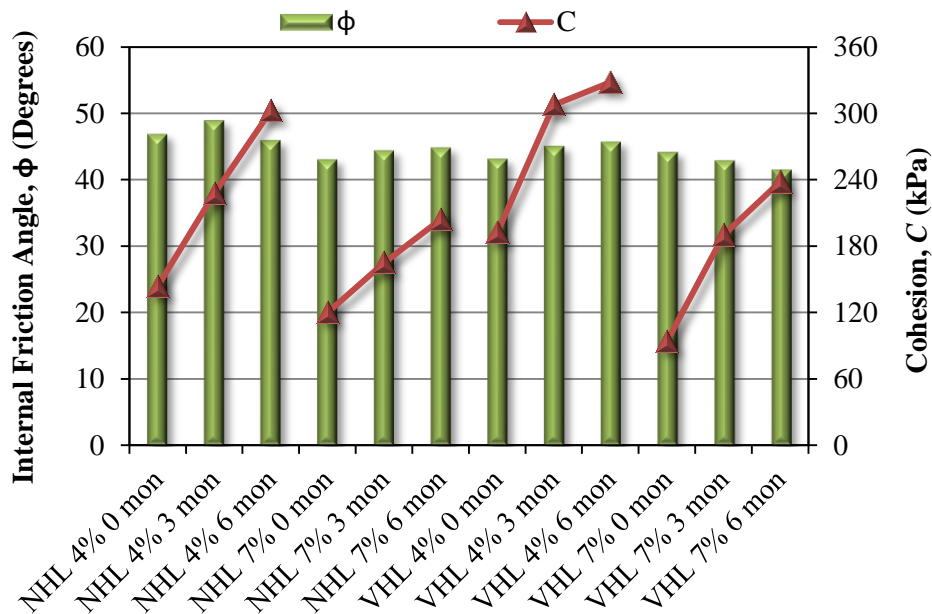
Figure 20. Cohesion and internal friction angle for different asphalt mixtures at 40°C.

As shown in Figure 19 and Figure 20, the slope of the GD-P yield surface (α) had an average value of 0.352 with a standard deviation of 0.016, and the internal friction angle (ϕ) had an average value of 45 degrees with a standard deviation of 2 degrees. Both α and ϕ had limited variations for the tested asphalt mixture specimens; thus, one can conclude that α and ϕ are not affected by the binder type, air void content, and aging period. This is reasonable since ϕ relies on the aggregate contacts and interlocks, which depend on the aggregate gradation of the asphalt mixture specimen. Since all of the tested asphalt mixture specimens had an identical gradation, it makes sense that ϕ remained similar for the different asphalt mixture specimens that were tested in this study. α represents the internal friction angle according to Equation 19; thus, α also stays close even though the asphalt mixture specimens have different binders, air void contents, and aging periods.

Figure 19 and Figure 20 also indicate that the intercept of the GD-P yield surface (κ_0) and cohesion (C) increased as the aging period increased or the air void content decreased. κ_0 and C of the asphalt mixture with Binder V were a little greater than the asphalt mixture with Binder N. Actually, κ_0 and C quantify the cohesive properties of the concrete. A stiffer asphalt mixture (e.g., due to stiffer binder, low air voids, longer aging periods) tends to have a greater cohesive strength. Based on the testing results, two relations between κ_0, C, and σ_y in the uniaxial compressive strength tests are regressed as follows:

$$C = 0.1973 \times \sigma_y + 16.22 \qquad R^2 = 0.9734 \tag{52}$$

$$\kappa_0 = 0.2102 \times \sigma_y + 20.93 \qquad R^2 = 0.9536 \tag{53}$$

Equations 52 and 53 demonstrate that κ_0 and C are highly related to the initial yield strength. By considering Equation 51 with Equations 52 and 53, one may conclude that a stiffer asphalt mixture tends to have higher values for κ_0 and C.

Figure 21 shows the measured values of the hardening parameters κ_1 and κ_2 for different asphalt mixtures. In general, κ_1 determines the amplitude of the strain hardening, and it increases as the air void content decreases or the aging period increases. In fact, κ_1, similar to κ_0, represents the cohesive properties of the asphalt mixture, and a stiffer asphalt mixture tends to have a greater κ_1. κ_2 determines the rate of the strain hardening for the asphalt mixture in

compression. Testing results in Figure 21 do not show obvious differences for κ_2 when asphalt mixtures have different binders, air void contents, and aging periods.
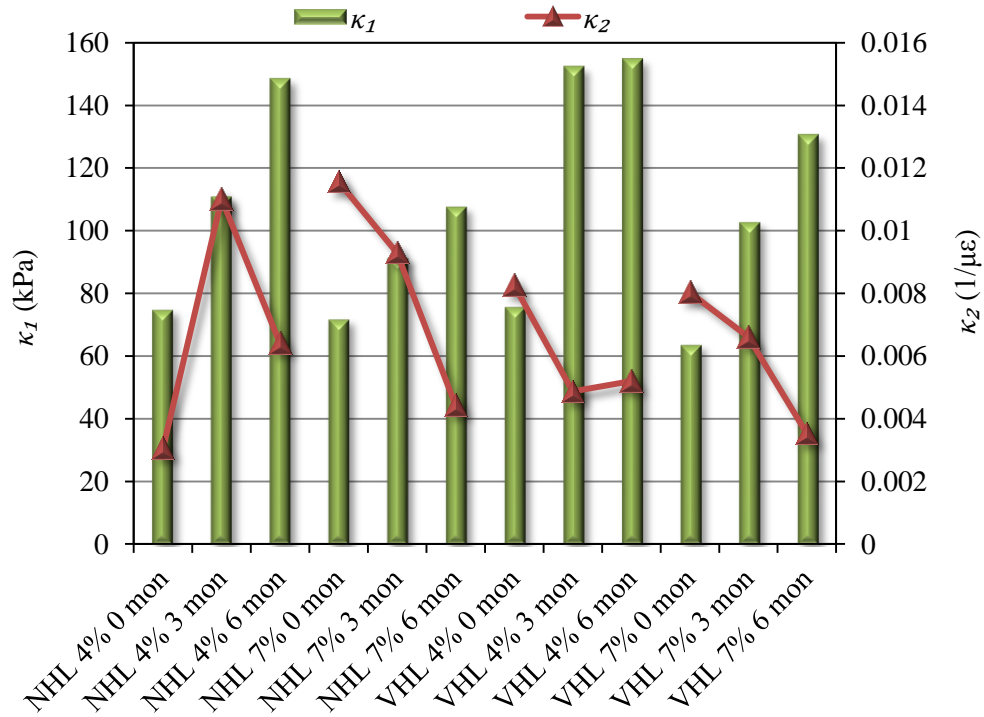
Figure 21. Strain hardening parameters κ_1 and κ_2 for different asphalt mixtures at 40°C.

Viscofracture Material Properties of Different Asphalt Mixtures

By applying the pseudo J-integral Paris' law to the axial and radial damage densities of the asphalt mixtures with different binders, air void contents, and aging periods, the material constants in the pseudo J-integral Paris' law were determined for different asphalt mixtures. Figure 22 shows the model coefficients of the axial pseudo J-integral Paris' law for different asphalt mixtures. As Figure 22 illustrates, A_1 decreased and n_1 increased when the asphalt mixture became stiffer, which might have been due to a stiffer binder, a lower air void content, and a longer aging period. This observation complies with Schapery's viscoelastic fracture theory (Schapery, 1984; Kuai et al., 2009) as well as the results in a preliminary study (Zhang et al., 2012c). Based on Schapery's theory, n_1 is inversely proportional to the slope of creep compliance, e.g., $n_1 = 1 + 1/m$, where m is the slope of the creep compliance that is modeled by $D(t) = D_0 + D_2 t^m$. It is known that a stiffer asphalt mixture normally has a smaller

44

value of m than a softer asphalt mixture. Thus, the stiffer asphalt mixture has a relatively larger n_1 value, which was verified by the testing results of this study.
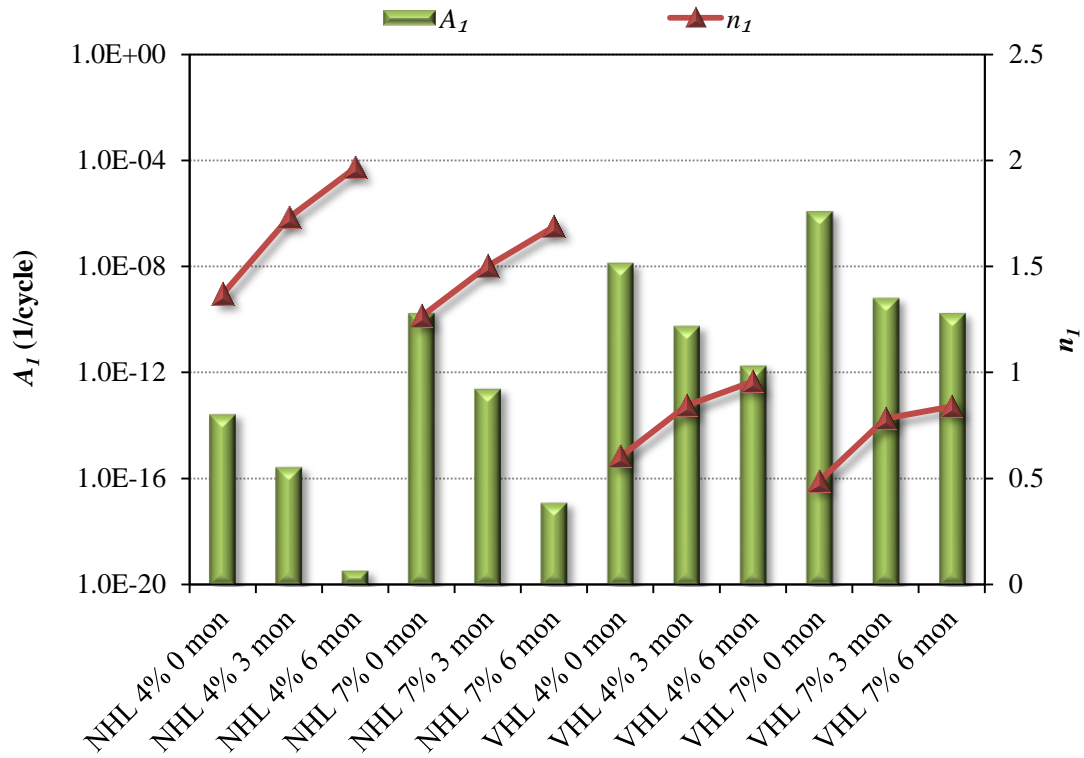
Figure 22. Viscofracture coefficients of axial pseudo J-integral Paris' law for different asphalt mixtures.

Figure 23 shows that A_2 decreased and n_2 increased when the asphalt mixture became stiffer, which was due to a longer aging period. However, the changes of A_2 and n_2 did not show consistent relations (e.g., A_2 decreased and n_2 increased) when the asphalt mixture had a lower air void content or used a stiffer binder. More theoretical analysis and laboratory tests are needed to investigate the factors that affect the values of A_2 and n_2 in asphalt mixtures.
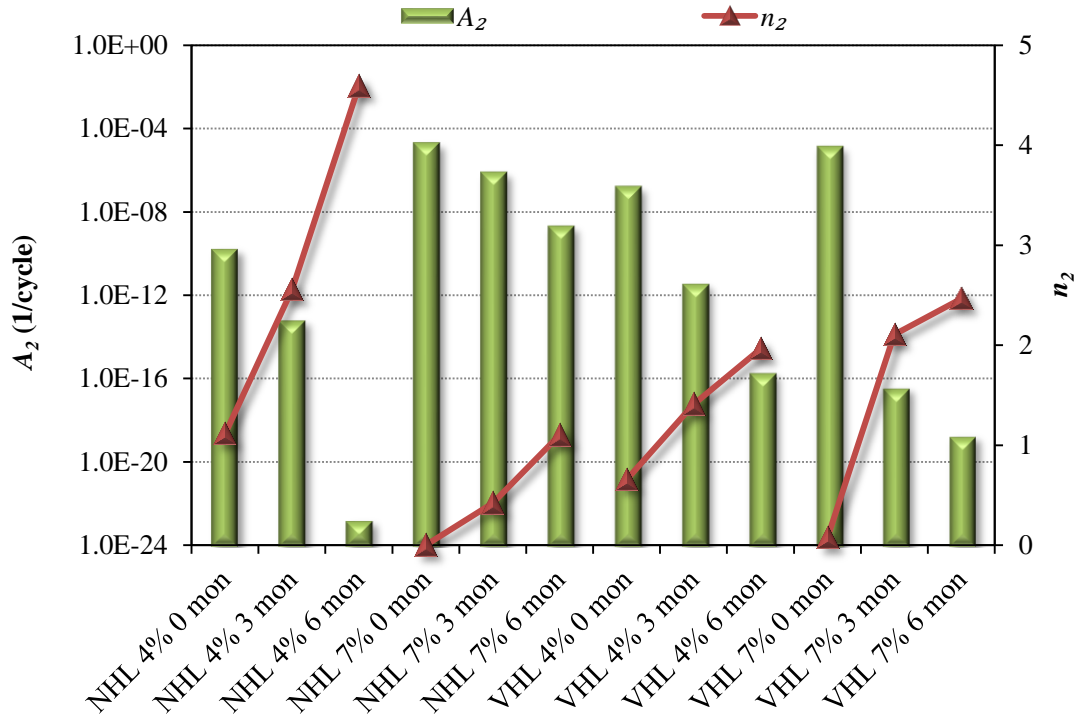
Figure 23. Viscofracture coefficients of radial pseudo J-integral Paris' law for different asphalt mixtures.

Based on the testing data in Figure 22 and Figure 23, linear relationships are found between $\log(A_i)$ and n_i with high values of coefficients of determination (R^2), which are shown in Figure 24. It must be noted that A_i indicates the initial cracking evolution speed and n_i indicates the increasing rate of the cracking evolution speed. Based on the testing results, it was found that a stiffer asphalt mixture tended to have a lower initial cracking evolution speed (A_i), which indicates a longer crack initiation period. The increasing rate of the cracking evolution speed (n_i) of the stiffer asphalt mixture was relatively high, which indicates a faster crack evolution and a shorter crack propagation period. This finding complies with the common laboratory observations for a stiff material that normally has brittle cracking. The asphalt mixture with a brittle cracking mode normally needs a longer period to initiate the cracks; however, the cracks will propagate at a relatively high speed once the material is cracked, and vice versa.
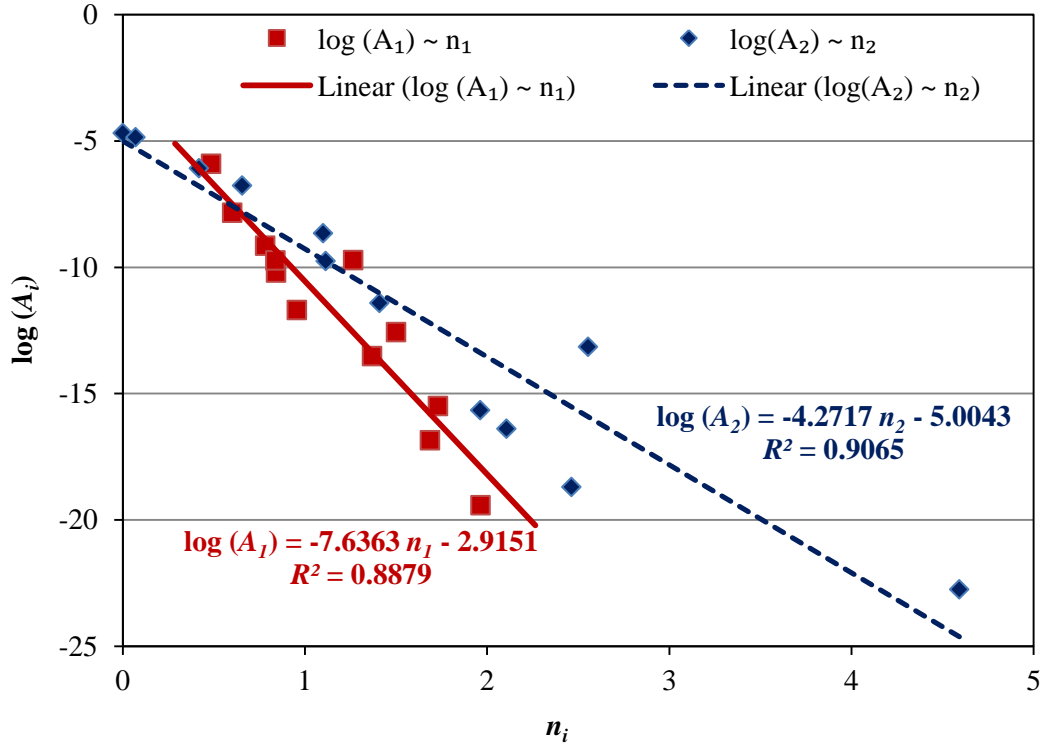
Figure 24. Relationships between A_i and n_i of pseudo J-integral Paris' law for asphalt mixtures.

Model Validations

Laboratory Validation Test

Octahedral shear strength tests at different normal and confining stresses were proposed to validate the proposed GD-P yield surface model on the octahedral plane for the asphalt concrete. The materials used in the mixture were Binder V and Hanson limestone. The aggregate gradation was Type C as specified by TxDOT procedure (2004). The optimum asphalt content was determined based on TxDOT specification (TxDOT, 2008) as 4.4 percent. The asphalt mixtures were compacted using a Superpave gyratory compactor at two target air void contents, namely 4 percent and 7 percent, respectively.

Figure 25 shows the octahedral shear test configuration. The tests were performed using a multi-directional direct simple shear testing device developed at Texas A&M University, and more information about the device can be found in the literature (Rutherford, 2012; Rutherford and Biscontin, 2013). The cylindrical specimen had a diameter of 100 mm and a height of 35 mm, which complies with a minimum length-to-height ratio of 3 (Weissman et al., 1999). A smaller size of the specimen was adopted in this test compared to the standard simple shear test

(SST), which uses 150 mm in diameter and 50 mm in height, in order to ensure that the maximum shear load was below the machine capacity. The specimens were glued between two end caps. The top end cap was attached using an assembly clamp to the machine axial loading platen that could apply the normal load (i.e., σ that is a normal stress in the axial direction of the specimen). The bottom end cap was attached to a horizontally moveable shear loading platen that could provide the shear load (i.e., τ that is a shear stress in the horizontal direction). The whole system was enclosed in a pressure chamber that could provide a constant air confining pressure (i.e., p that was a confining pressure in all directions).
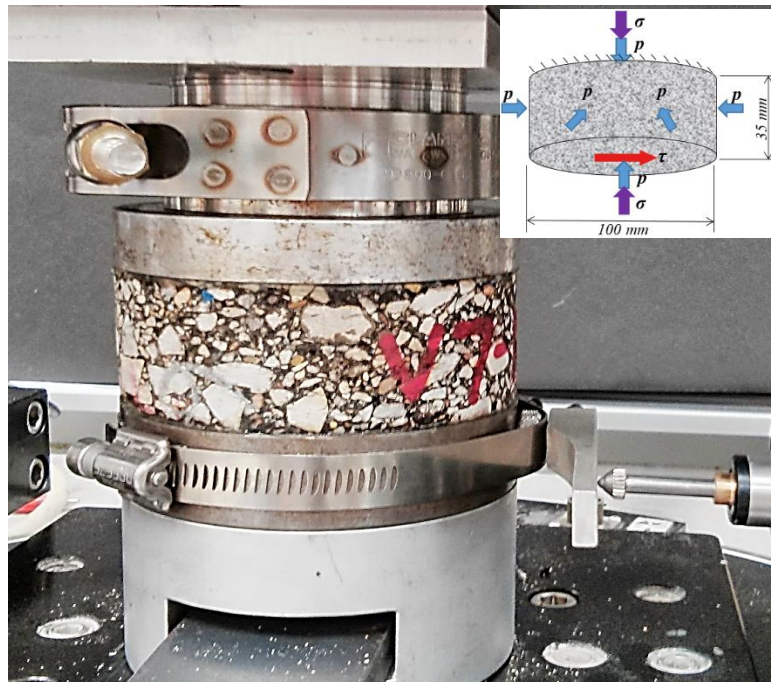
Figure 25. Shear validation test configuration and loading modes.

To evaluate the shear yield stress on the octahedral plane, the first stress invariant (i.e., $I_1 = \sigma_{kk} = \sigma_{11} + \sigma_{22} + \sigma_{33}$) needed to remain constant during the shearing process. In this test, the stress state of the specimen was expressed as:

$$\sigma_{ij} = \begin{bmatrix} \sigma+p & \tau & 0 \\ \tau & p & 0 \\ 0 & 0 & p \end{bmatrix} \tag{54}$$

Thus, $I_1 = \sigma + 3p$ was controlled at 400 kPa by applying seven different p and σ levels, which are shown as levels A, B, C, D, E, F, and G in Table 5. In each test level, p and σ remained unchanged, and the shear load was increased at a constant shear strain rate of

286 µε/sec corresponding to a shear displacement rate of 0.01 mm/sec. An LVDT was used to record the horizontal shear displacement, which was also compared with the machine deformation. The shear load was applied on the specimen at a constant temperature of 50°C until the material ruptured or significant cracks were observed. The shear stress (i.e., τ in Equation 54) was determined as the initial yield stress using the stress-pseudostrain method proposed by the authors (Zhang et al., 2013). At least two replicates were tested for each stress level, and a third replicate was tested if a high variation was observed. Table 5 includes the average measured shear yield stress for each stress level.

Table 5. Test Parameters and Results of the Octahedral Shear Strength Test.

Materials and Test Parameters		Stress Case No.	Confining Pressure	Normal Load	Average Measured Yield Shear Stress	
			p	σ	τ @ 4%	τ @ 7%
Air Voids	4%					
	7%		kPa	kPa	kPa	kPa
Binder	PG 64-16	A	0	400	230	190
Aggregate	Limestone	B	33	300	250	205
I_1	400 kPa	C	67	200	255	225
Shear rate	286 µε/sec (0.01 mm/sec)	D	100	100	255	220
		E	133	0	237	220
Temperature	50°C	F	167	-100	220	195
Replicates	2	G	200	-200	195	160

Yield Surface Validation

The yield shear stress data for all tested asphalt concrete specimens were employed to compare the widely used ED-P model (which has similar yield surface as GD-P but employs a different function for $\rho(\theta')$ and $\rho(\theta') = \frac{1}{2}\left[1 + \frac{1}{d} + \left(1 - \frac{1}{d}\right)\cos(3\theta')\right]$) and the proposed GD-P (e.g., Equations 15 and 17) and to validate the latter. To plot the yield surface on the octahedral plane, the following stress invariants were calculated based on the measurements of σ, p, and τ:

$$\begin{cases} I_1 = \sigma_{kk} = \sigma + 3p \\ J_2 = \frac{1}{2}S_{ij}S_{ji} = \frac{1}{3}\sigma^2 + \tau^2 \\ J_3 = \det\left(S_{ij}\right) = \frac{2}{27}\sigma^3 + \frac{1}{3}\sigma\tau^3 \end{cases} \tag{55}$$

Then, the Lode angle (θ') was calculated according to Equation 16, and the distance between a yield point and the coordinate origin on the octahedral plane was the yield octahedral shear stress that was determined as $\tau_{oct} = \sqrt{2J_2}$. Thus, the horizontal and vertical coordinates of a yield point on a rectangular coordinate were calculated by $\tau_{oct}\sin\theta$ and $\tau_{oct}\cos\theta$, respectively. Based on this method, the yield points on the octahedral plane were plotted as the circle points in Figure 26 and Figure 27, which represent the yield octahedral shear stresses for the asphalt concrete with 4 percent and 7 percent air void contents, respectively. The predicted yield octahedral shear stresses were calculated using an internal friction angle of 44 degrees and the corresponding value of d as 0.62 based on the results in Table 4.

In Figure 26 and Figure 27, σ_1 stands for compression and $-\sigma_3$ stands for extension. A, B, C, D, E, F, and G represent different stress combinations of the normal stress and the confining pressure. One can find from both Figure 26 and Figure 27 that the predictions of the GD-P yield surface model matched well with the experimentally determined yield octahedral shear stresses, while the widely used ED-P model over-predicted the yield stresses on the octahedral plane. The reason for this finding is that the ED-P model produces a non-convex yield surface when the material internal friction angle exceeds 22 degrees; thus, the ED-P model is not applicable to characterize the yield surface of asphalt concrete that normally has a friction angle greater than 22 degrees. The proposed GD-P model is an inherently convex yield surface model over the full range of the internal friction angles from 0 to 90 degrees, which is a proper yield surface model for the asphalt mixtures.

The over-prediction of the yield shear stress of the ED-P model can put the rutting performance prediction in danger, as the rutting depth will be underestimated in an asphalt pavement analysis. Based on the results shown in Figure 26 and Figure 27, the asphalt mixtures of the field pavements will yield at a lower shear stress and start to develop permanent deformation earlier than the ED-P model prediction. Then, an under-predicted rutting depth is provided if using the ED-P model in the constitutive analysis of the asphalt pavements. Therefore, in the interest of the safety of the traveling public against wet-weather accidents, it is

emphatically recommended to employ the GD-P yield surface model rather than the ED-P model in the viscoplastic analysis of asphalt concrete.
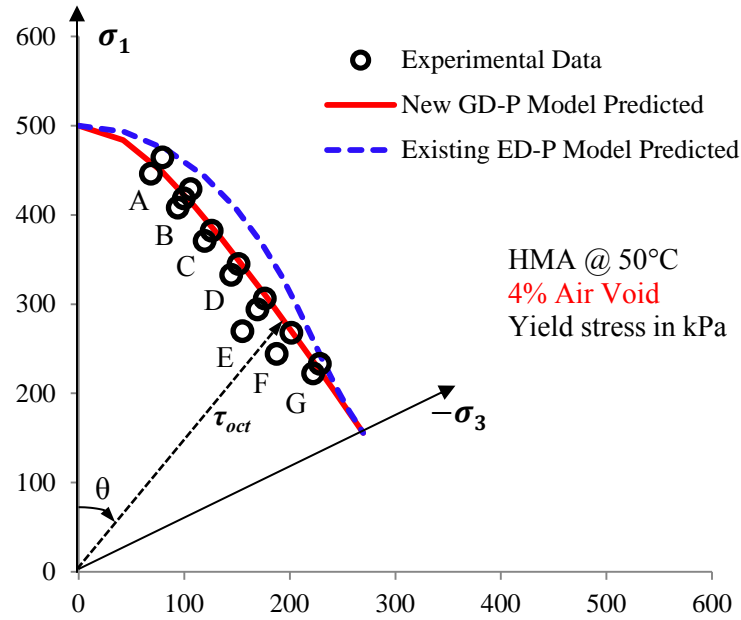
Figure 26. Comparisons of yield octahedral shear stresses between experimental data and the GD-P and ED-P model predictions for asphalt concrete with 4 percent air void content.
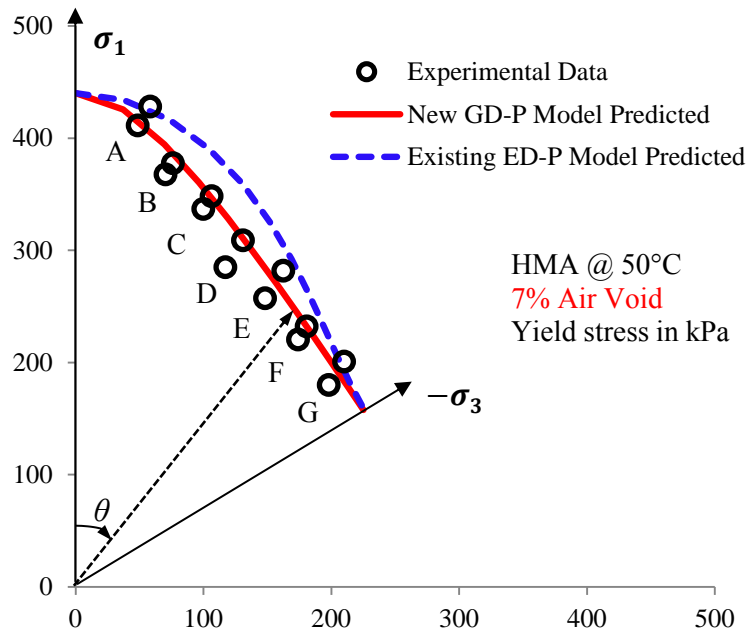
Figure 27. Comparisons of yield octahedral shear stresses between experimental data and the GD-P and ED-P model predictions for asphalt concrete with 7 percent air void content.

Yield Strength Validation

Since the proposed GD-P yield surface coincides with the apices of the Mohr-Coulomb yield surface, the relationship between α and ϕ in Equation 19 also applies to the GD-P yield surface. Using the measured ϕ, α is predicted by Equation 19 and compared with the measured α. A good agreement is found in Figure 28 between the measured α and the predicted α. Similarly, the relationship between κ_0, C, and ϕ in Equation 20 can also be applied to the GD-P model. Using the measured C and ϕ, κ_0 is predicted by Equation 20 and compared with the measured κ_0. A good agreement is shown in Figure 29 between the measured κ_0 and the predicted κ_0, which demonstrates that the relationship between C, ϕ, and κ_0 in Equation 20 also applies to the proposed GD-P yield surface.
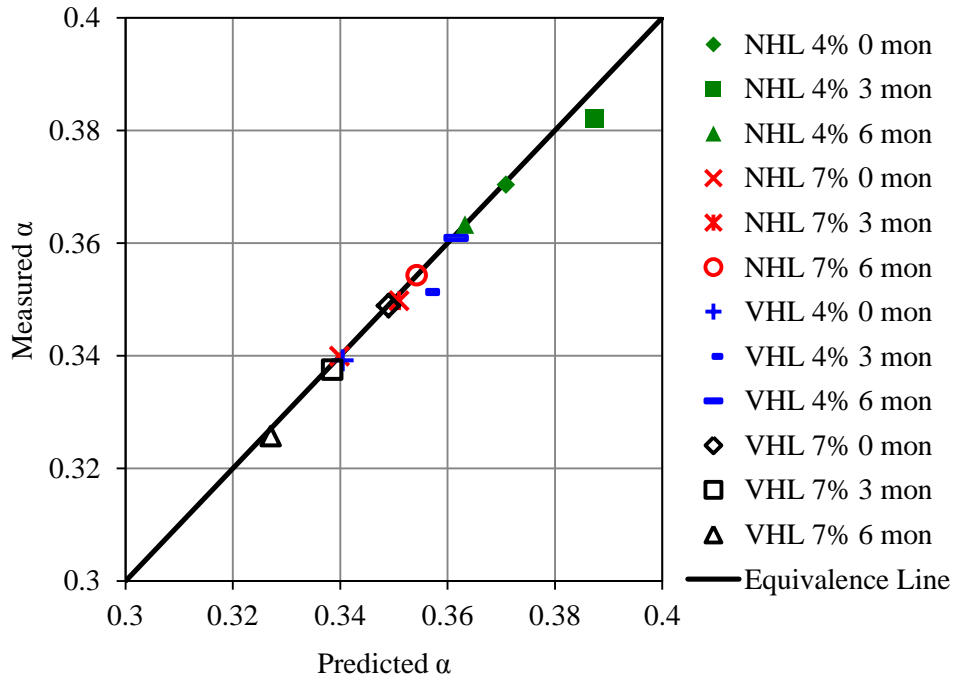
Figure 28. Comparisons between measured *α* from tests and predicted *α* based on *Φ* for different asphalt mixtures.
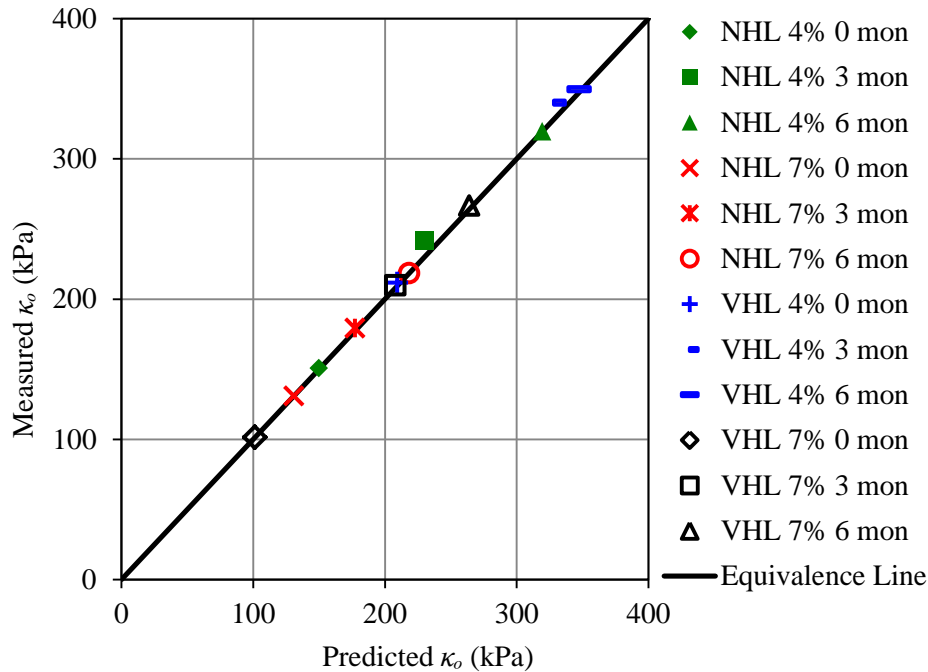
Figure 29. Comparisons between measured κ_0 from tests and predicted κ_0 based on C and Φ for different asphalt mixtures at 40°C.

The relationships between α, κ_0, C, and ϕ in Equations 19 and 20 are verified by Figure 28 and Figure 29. This finding can be used to simplify the testing protocols that are used to determine the model parameters. The TCS tests in Table 2 can be employed to perform strength tests at different confining pressures and determine the strength parameters such as α, κ_0, C, and ϕ. However, the TCS tests require testing equipment that can provide confinement during the tests, such as the RaTT cell used in this study or the triaxial cell used in the Material Testing System (MTS) machine. The equipment might not be accessible since it is relatively expensive, and the operations are more complicated compared to the uniaxial tests. To avoid these problems, users can employ the indirect tensile strength (IDT) test as an alternative for the TCS test. In fact, some studies (Christensen et al., 2004; Pellinen et al., 2005) showed that the Mohr-Coulomb strength parameters (C and ϕ) could be determined by performing UCS and IDT strength tests. Once C and ϕ are determined, the model parameters α and κ_0 can be directly calculated by Equations 19 and 20.

5. SUMMARIES AND CONCLUSIONS

A comprehensive characterization of asphalt concrete was accomplished in this project by constitutively modeling the anisotropy and viscoelasticity of undamaged asphalt mixtures and the viscoplasticity and viscofracture of damaged asphalt mixtures. The research findings resulting from this project are summarized below.

Research Findings

The permanent deformation (rutting) of asphalt concrete was intensively characterized by a modified Perzyna's anisotropic viscoplastic-fracture model. The development of the model led to the following material properties and conclusions:

- A modified effective stress was employed in the formulation of the model to account for both the inherent anisotropy due to the aggregates' orientation and the crack-induced anisotropy caused by the crack growth. The permanent deformation of the asphalt pavement would be underestimated if the anisotropy were not included in the viscoplastic modeling of the asphalt mixture.

- A GD-P yield surface was developed to provide a smooth and convex yield surface and to address the cohesion and internal friction of the material. The GD-P model can characterize the full range of the internal friction angles from 0 to 90 degrees. In contrast, the widely used ED-P model was found to be applicable only for a material that has an internal friction angle less than 22 degrees due to the convexity criterion of the yield surface.

- A non-associated flow rule was used for the viscoplastic potential to address the volumetric dilation of asphalt mixtures. The slope of the viscoplastic potential surface was found to be solely dependent on the inherent anisotropy of the asphalt mixtures.

- A temperature- and strain rate-dependent strain hardening function was proposed in the GD-P model. The results of the strength tests at different temperatures and strain rates indicated that a stiffer asphalt concrete had greater cohesion and strain hardening amplitude, both of which declined as temperature increased or strain rate decreased. The temperature and strain rate factors of the yield surface can be accurately determined solely by the peak stress of the strength tests.

- A pseudo J-integral based Paris' law in terms of damage density was proposed to characterize the evaluation of the viscofracture cracking of asphalt mixtures under a compressive destructive load. The material constants in the Paris' law were determined and found to be highly correlated. Consistent results were obtained for different asphalt mixtures; for instance, a stiffer asphalt mixture was demonstrated to have a higher modulus, a lower phase angle, a greater flow number, and a larger n_1 value (exponent of Paris' law).

A systematic laboratory testing protocol was proposed to determine the model parameters and the material properties of the undamaged and damaged asphalt mixtures. The testing methods used in this study (see Table 1 and Table 2) were very effective and efficient for the determination of the model parameters and material properties. A brief review of the test protocol and the efficiency of each characterizing test is as follows:

- Inherent anisotropy: the lateral surface scanning (hot-dog) tests utilize a portable scanner and a rotating device to obtain the image of the aggregates with a high resolution and can be finished within 5 min.
- Viscoelasticity: nondestructive uniaxial compressive creep (UCC) tests can be accomplished in any common material testing machine that can provide a constant axial load and record the axial deformation. This test can also be finished within 5 min.
- Viscoplasticity (Perzyna's viscosity) and viscofracture: the nondestructive dynamic modulus (NDM) and destructive dynamic modulus (DDM) tests are uniaxial tests and can be performed on any common material testing machine that can provide a sinusoidal repeated axial load and record the axial and radial deformation. The NDM tests need about 15 min, and the DDM can be finished within 2 h for most of the asphalt mixtures at relatively high temperatures (e.g., $\geq 40°C$).
- Viscoplasticity (yielding and strain hardening): the uniaxial compressive strength (UCS) test is performed on the same machine as the UCC test with the same testing configuration. The triaxial compressive strength (TCS) needs a triaxial cell or RaTT cell; however, as discussed in the last chapter, the TCS test can be replaced by the indirect tensile strength test, which only requires the same testing machine as the UCC test. Each of the strength tests can be finished within 5 min.

To account for the temperature effect on the material properties, the aforementioned tests, such as the UCC test, UCS test, and DDM test, might need to be performed at several different temperatures. To reach the equilibrium temperature, it is common to take 2 or 3 h to change from one temperature to another. In summary, by using the mechanistic models and testing protocol proposed in this study, it is possible to characterize one type of the asphalt mixture in compression and obtain all the material properties and model parameters within 1 day. The constitutive models developed for the characterization of asphalt concrete in compression can be effectively implemented for the rutting prediction of the asphalt pavements under a variety of traffic, structural, and environmental conditions.

Recommendations for Future Work

The work done in this study is a first and basic step to a successful prediction of the field performance of asphalt pavements. More studies are recommended as continuations of this study.

The mechanistic models proposed in this study need to be implemented in the performance prediction of asphalt pavements. The evolutionary rules for the viscoplastic and viscofracture deformation need to be formulated in incremental expressions, which are used in the numerical finite and boundary element predictions of pavement distresses.

More work can be done in the prediction of the field performance of asphalt pavements at different traffic loads, environmental conditions, and pavement structures. Comparisons between the predictions and field measurements are also necessary to evaluate the accuracy of the constitutive models.

Because the test protocol used in this project produces measured material properties, a systematic program of measuring and cataloging the properties of the most commonly used mixture properties can now be initiated. Once it is developed and available to pavement designers, this catalog will make the process of mixture design and performance prediction much more efficient.

The testing protocol—being simple, rapid, and efficient—can now be used to measure the effects of moisture vapor, healing, additives, and modifiers on the properties of commonly used asphalt mixtures. The characteristics of the warm mix asphalt mixtures can now be compared objectively with the same properties of the hot mix asphalt mixtures.

REFERENCES

Abdulshafi, A., and Majidzadeh, K. (1984). "Combo viscoelastic-plastic modeling and rutting of asphalt mixtures." *Transportation Research Record: Journal of the Transportation Research Board*, No. 968, Transportation Research Board of the National Academies, Washington, DC, 19-31.

Abu Al-Rub, R. K., Darabi, M. K., Huang, C.-W., Masad, E. A., and Little, D. N. (2012). "Comparing finite element and constitutive modeling techniques for predicting rutting of asphalt pavements." *International Journal of Pavement Engineering*, 13(4), 322-338.

Bardet, J. P. (1990). "Lode dependences for isotropic pressure-sensitive elastoplastic materials." *Journal of Applied Mechanics*, 57(3), 498-506.

Chehab, G. R., Kim, Y. R., Schapery, R. A., Witczak, M. W., and Bonquist, R. (2003). "Characterization of asphalt concrete in uniaxial tension using a viscoelastoplastic continuum damage model." *Journal of the Association of Asphalt Paving Technologists*, 72, 315-355.

Chen, W. F., and Han, D. J. (1988). *Plasticity for structural engineers*, Springer, New York, NY.

Christensen, D. W., Bonaquist, R., Anderson, D. A., and Gokhale, S. (2004). "Indirect tension strength as a simple performance test." *New Simple Performance Tests for Asphalt Mixes*, E-Circular, Transportation Research Board of The National Academies, Washington, DC, 44-57.

Darabi, M. K., Abu Al-Rub, R. K., Masad, E. A., Huang, C.-W., and Little, D. N. (2011). "A thermo-viscoelastic-viscoplastic-viscodamage constitutive model for asphaltic materials." *International Journal of Solids and Structures*, 48(1), 191-207.

Drescher, A., Kim, J. R., and Newcomb, D. E. (1993). "Permanent deformation in asphalt concrete." *Journal of Materials in Civil Engineering*, 5(1), 112-128.

Florea, D. (1994a). "Associated elastic/viscoplastic model for bituminous concrete." *International Journal of Engineering Science*, 32(1), 79-86.

Florea, D. (1994b). "Nonassociated elastic viscoplastic model for bituminous concrete." *International Journal of Engineering Science*, 32(1), 87-93.

Gibson, N. H., Schwartz, C. W., Schapery, R. A., and Witczak, M. W. (2003). "Viscoelastic, viscoplastic, and damage modeling of asphalt concrete in unconfined compression." *Transportation Research Record: Journal of the Transportation Research Board*, No. 1860, Transportation Research Board of the National Academies, Washington, DC, 3-15.

Huang, C.-W., Masad, E., Muliana, A. H., and Bahia, H. (2007). "Analysis of nonlinear viscoelastic properties of asphalt mixtures." *Symposium on Mechanics of Flexible Pavements at the 15th U.S. National Congress of Theoretical and Applied Mechanics*, American Society of Civil Engineers, Boulder, CO, 64-72.

Kachanov, L. M. (1986). *Introduction to continuum damage mechanics*, Springer, New York, NY.

Kuai, H., Lee, H., Zi, G., and Mun, S. (2009). "Application of generalized J-integral to crack propagation modeling of asphalt concrete under repeated loading." *Transportation Research Record: Journal of the Transportation Research Board*, No. 2127, Transportation Research Board of the National Academies, Washington, DC, 72-81.

Lemaitre, J., and Desmorat, R. (2005). *Engineering damage mechanics: Ductile, creep, fatigue and brittle failures*, Springer, New York, NY.

Levenberg, E., and Uzan, J. (2004). "Triaxial small-strain viscoelastic-viscoplastic modeling of asphalt aggregate mixes." *Mechanics of Time-Dependent Materials*, 8(4), 365-384.

Lu, Y., and Wright, P. J. (1998). "Numerical approach of visco-elastoplastic analysis for asphalt mixtures." *Computers & Structures*, 69(2), 139-147.

Mahboub, K. (1990). "Asphalt concrete creep as related to rutting." *Journal of Materials in Civil Engineering*, 2(3), 147-163.

Masad, E., Dessouky, S., and Little, D. (2007). "Development of an elastoviscoplastic microstructural-based continuum model to predict permanent deformation in hot mix asphalt." *International Journal of Geomechanics*, 7(2), 119-130.

Masad, E., Huang, C.-W., Airey, G., and Muliana, A. (2008). "Nonlinear viscoelastic analysis of unaged and aged asphalt binders." *Construction and Building Materials*, 22(11), 2170-2179.

Masad, E., Muhunthan, B., Shashidhar, N., and Harman, T. (1998). "Aggregate orientation and segregation in asphalt concrete." *Application of geotechnical principles in pavement engineering*, A. T. Papagiannakis, and C. W. Schwartz, eds. Boston, MA, 69-80.

Nguyen, D. T., Nedjar, B., and Tamagny, P. (2007). "Cyclic elasto-viscoplastic model for asphalt concrete materials." *Road Mater. Pavement Des.*, 8(2), 239-255.

Oda, M. (1993). "Inherent and induced anisotropy in plasticity theory of granular soils." *Mechanics of Materials*, 16(1-2), 35-45.

Oda, M., and Nakayama, H. (1989). "Yield function for soil with anisotropic fabric." *Journal of Engineering Mechanics*, 115(1), 89-104.

Pellinen, T. K., Xiao, S., Carpenter, S., Masad, E., Di Benedetto, H., and Roque, R. (2005). "Relationship between triaxial shear strength and indirect tensile strength of hot mix asphalt." *Journal of the Association of Asphalt Paving Technologists*, 74, 347-379.

Perl, M., Uzan, J., and Sides, A. (1983). "Visco-elasto-plastic constitutive law for a bituminous mixture under repeated loading." *Transportation Research Record: Journal of the Transportation Research Board*, No. 911, Transportation Research Board of the National Academies, Washington, DC, 20-27.

Perzyna, P. (1971). "Thermodynamic theory of viscoplasticity." *Advances in Applied Mechanics*, 11, 313-354.

Pickering, D. J. (1970). "Anisotropic elastic parameters for soil." *Geotechnique*, 20(3), 271-276.

Qi, X., and Witczak, M. W. (1998). "Time-dependent permanent deformation models for asphaltic mixtures." *Transportation Research Record*, No. 1639, Transportation Research Board of the National Academies, Washington, DC, 83-93.

Rabotnov, Y. N. (1969). *Creep problems in structural members*, North-Holland, Amsterdam, the Netherlands.

Ramsamooj, D. V., and Ramadan, J. (1999). "Prediction of permanent deformation of asphalt concrete in cyclic and monotonic loading." *Journal of Testing and Evaluation*, 27(5), 320-326.

Rutherford, C. J. (2012). "Development of a multi-directional direct simple shear testing device for characterization of the cyclic shear response of marine clays." Texas A&M University, College Station, TX.

Rutherford, C. J., and Biscontin, G. (2013). "Development of a multi-directional simple shear testing device." *Geotechnical Testing Journal*, Accepted for publication.

Saadeh, S., Masad, E., and Little, D. (2007). "Characterization of asphalt mix response under repeated loading using anisotropic nonlinear viscoelastic-viscoplastic model." *Journal of Materials in Civil Engineering*, 19(10), 912-924.

Schapery, R. A. (1969). "On the characterization of nonlinear viscoelastic materials." *Polymer Engineering & Science*, 9(4), 295-310.

Schapery, R. A. (1984). "Correspondence principles and a generalized J-integral for large deformation and fracture analysis of viscoelastic media." *International Journal of Fracture*, 25(3), 195-223.

Schapery, R. A. (1997). "Nonlinear viscoelastic and viscoplastic constitutive equations based on thermodynamics." *Mechanics of Time-Dependent Materials*, 1(2), 209-240.

Schapery, R. A. (1999). "Nonlinear viscoelastic and viscoplastic constitutive equations with growing damage." *International Journal of Fracture*, 97(1-4), 33-66.

Schwartz, C. W., Gibson, N. H., Schapery, R. A., and Witczak, M. W. (2004). "Viscoplasticity modeling of asphalt concrete behavior." *Proc., Recent Advances in Materials Characterization and Modeling of Pavement Systems*, American Society of Civil Engineers, 144-159.

Seibi, A., Sharma, M., Ali, G., and Kenis, W. (2001). "Constitutive relations for asphalt concrete under high rates of loading." *Transportation Research Record: Journal of the Transportation Research Board*, No. 1767, Transportation Research Board of the National Academies, Washington, DC, 111-119.

Sousa, J. B., and Weissman, S. L. (1994). "Modeling permanent deformation of asphalt-aggregate mixes." *Journal of Association of Asphalt Paving Technologists*, 63, 224-257.

Sousa, J., Weissman, S. L., Sackman, J. L., and Monismith, C. L. (1993). "A nonlinear elastic viscous with damage model to predict permanent deformation of asphalt concrete mixtures." *Transportation Research Record: Journal of the Transportation Research Board*, No. 1384, Transportation Research Board of the National Academies, Washington, DC, 80-93.

Sullivan, R. (2008). "Development of a viscoelastic continuum damage model for cyclic loading." *Mechanics of Time-Dependent Materials*, 12(4), 329-342.

Tan, S.-A., Low, B.-H., and Fwa, T.-F. (1994). "Behavior of asphalt concrete mixtures in triaxial compression." *Journal of Testing and Evaluation*, 22(3), 195-203.

Tashman, L., Masad, E., Little, D., and Zbib, H. (2005). "A microstructure-based viscoplastic model for asphalt concrete." *International Journal of Plasticity*, 21(9), 1659-1685.

Tashman, L., Masad, E., Peterson, B., and Saleh, H. (2002). "Internal structure analysis of asphalt mixes to improve the simulation of Superpave gyratory compaction to field conditions." *Journal of Association of Asphalt Paving Technologists*, 70, 605-645.

Tobita, Y. (1989). "Fabric tensors in constitutive equations for granular materials." *Soils and Foundations*, 29(4), 91-104.

Tobita, Y., and Yanagisawa, E. (1988). "Contact tensor in constitutive model for granular materials." *Micromechanics of granular materials*, M. Satake, and J. T. Jenkins, eds., Elsevier Science Publishers B.V., Amsterdam, The Netherlands, 263-270.

Tobita, Y., and Yanagisawa, E. (1992). "Modified stress tensors for anisotropic behavior of granular materials." *Soils and Foundations*, 32(1), 85-99.

TxDOT (2004). "Standard specifications for construction and maintenance of highways, streets, and bridges." Texas Department of Transportation, Austin, TX.

TxDOT (2008). "Test procedure for design of bituminous mixtures." *TxDOT Designation: Tex-204-F*, Texas Department of Transportation, Austin, TX.

Uzan, J. (1996). "Asphalt concrete characterization for pavement performance prediction." *Journal of Association of Asphalt Paving Technologists*, 65, 573-607.

Weissman, S. L., Harvey, J., Sackman, J. L., and Long, F. (1999). "Selection of laboratory test specimen dimension for permanent deformation of asphalt concrete pavements." *Transportation Research Record: Journal of the Transportation Research Board*, Transportation Research Board of the National Academies, Washington, DC, 113-120.

Yang, Z. X., Lit, X. S., and Yang, J. (2008). "Quantifying and modeling fabric anisotropy of granular soils." *Geotechnique*, 58(4), 237-248.

Zhang, Y., Luo, R., and Lytton, R. L. (2011). "Microstructure-based inherent anisotropy of asphalt mixtures." *Journal of Materials in Civil Engineering*, 23(10), 1473-1482.

Zhang, Y., Luo, R., and Lytton, R. L. (2012a). "Anisotropic viscoelastic properties of undamaged asphalt mixtures." *Journal of Transportation Engineering*, 138(1), 75-89.

Zhang, Y., Luo, R., and Lytton, R. L. (2012b). "Characterizing permanent deformation and fracture of asphalt mixtures by using compressive dynamic modulus tests." *Journal of Materials in Civil Engineering*, 24(7), 898-906.

Zhang, Y., Luo, R., and Lytton, R. L. (2012c). "Mechanistic modeling of fracture in asphalt mixtures under compressive loading." *Journal of Materials in Civil Engineering*, 25(9), 1189-1197.

Zhang, Y., Luo, R., and Lytton, R. L. (2013). "Characterization of viscoplastic yielding of asphalt concrete." *Construction and Building Materials*, 47, 671-679.